31-109-38-2831—2 TR
MITNE-156

TRANSIENT HEAT TRANSFER INDUCED PRESSURE FLUCTUATIONS IN THE FUEL COOLANT INTERACTION

by

Charles E. Watson

August, 1973

Department of Nuclear Engineering
Massachusetts Institute of Technology
77 Massachusetts Avenue
Cambridge, Massachusetts 02139

AEC Research and Development
Contract 31-109-38-2831
Argonne National Laboratory

MIT Libraries
Document Services

Room 14-0551
77 Massachusetts Avenue
Cambridge, MA 02139
Ph: 617.253.2800
Email: docs@mit.edu
http://libraries.mit.edu/docs

DISCLAIMER OF QUALITY

Due to the condition of the original material, there are unavoidable flaws in this reproduction. We have made every effort possible to provide you with the best copy available. If you are dissatisfied with this product and find it unusable, please contact Document Services as soon as possible.

Thank you.

The images contained in this document are of the best quality available.

TRANSIENT HEAT TRANSFER INDUCED PRESSURE FLUCTUATIONS IN THE FUEL COOLANT INTERACTION

by

Charles E. Watson

August, 1973

Department of Nuclear Engineering
Massachusetts Institute of Technology
77 Massachusetts Avenue
Cambridge, Massachusetts 02139

Approved

Neil E. Todreas
Principal Investigator

TRANSIENT HEAT TRANSFER INDUCED PRESSURE FLUCTUATIONS IN THE FUEL COOLANT INTERACTION

ABSTRACT

Rapid generation of high pressures and mechanical work may result when thermal energy is transferred from the hot molten nuclear fuel to the coolant in an LMFBR accident. Such energetic thermal interactions can happen if a large heat transfer area is created by the fragmentation of the molten fuel in the coolant.

A model was developed by Kazimi to simulate the dynamic growth of the vapor film around a hot spherical particle which was suddenly immersed in a coolant. The present work extends this model to give the pressure fluctuations on the interior and exterior due to the surface pressure of the vapor film as a driving function.

In this work the acoustic wave equation for a fluctuating pressure is developed for a compressible, viscous fluid. This equation is solved by the Fourier transform technique analytically and the finite fast Fourier transform algorithm is used numerically to obtain the pressure as a function of time. These techniques are applied to various cases of hot spheres in water to determine if a previously advanced hypothesis of cavitation is a principal mechanism in inducing cavitation and a subsequent fragmentation of the hot molten material in water. In some cases there is a good correlation with the negative pressure trends and the known fragmentation behavior.

ACKNOWLEDGEMENTS

I wish to express my sincere appreciation to Professor Neil E. Todreas for his encouragement, suggestions and care in the development of this work. I also wish to thank Professor David D. Lanning and Professor Warren M. Rohsenow for their advice during the later stages of development of this model.

I am also grateful to Miss Cindi Mitaras for her careful and efficient typing of the manuscript.

Finally, I want to express my gratitude to my wife who has worked hard to enable me to go to school again and whose love and encouragement has sustained me in a harsh and hostile environment (Boston).

TABLE OF CONTENTS

LIST OF FIGURES AND TABLES

CHAPTER I

INTRODUCTION

CHAPTER I

INTRODUCTION

I.1 Introduction

Small scale laboratory experiments and TREAT[1] experiments have shown that UO_2 fragments as it comes into contact with liquid sodium. Other experience[2] has shown that violent explosions can occur if large masses of molten metal come into sudden contact with a coolant (water in many cases). These experiments are quite convincing in showing that the large rapid energy releases are not due to chemical reactions but instead are the result of large total heat transfer rates caused possibly by extensive fragmentation to expose a large heat transfer area. The subsequent high pressure can be assessed in detail by direct measurement and by establishing models.

It is important to understanding fragmentation to calculate both interior and exterior pressure for the molten globule. Since the extent of fragmentation lies much further down a long chain of events which are not well understood, we can hope that by starting to investigate the parts of the chain where our knowledge of the physics involved is reasonably secure, it will be possible to unravel the rest of the problem. One useful result might be to establish a correlation between the pressure history and the extent of

fragmentation. This is useful because we can make a model calculation for the pressure history and then use limited experimental data to extend predictions of fragmentation to previously unmeasured cases. We are led to expect this connection by a suggestion due to Kazimi[3] that the mechanism for fragmentation under certain conditions is cavitation of the hot material during a subatmospheric pressure swing (below the vapor pressure for the hot liquid) at the surface of the drop.

The film pressure at the surface can be obtained from a model due to Kazimi[3]. The film pressure obtained in this way can be used to calculate the interior pressure waves starting from a given film pressure in order to investigate the possibility of cavitation as a mechanism for inducing fragmentation. It is clear, however, that any detailed model of fragmentation will give the film pressure as a function of time and can be compared to these experimental results.

I.2 A Fragmentation Model

A review by Kazimi[3] of the fragmentation experiments that have been performed in recent years has shown the following overall characteristics.

1. When the molten material is at a temperature lower than the boiling point of the coolant, fragmentation may occur and will follow a pattern predicted by hydrodynamic effect (Weber number effect).
2. At higher temperatures, the fragmentation is dependent on the temperatures of both the molten material and coolant.
3. Different hot materials dropped into the same cold liquid may result in different fragmentation behavior (e.g., at 600°C Sn fragments in water at 30°C while Zn does not).

The first and second point taken together suggest a competition between hydrodynamic and thermal effects. The third point suggests that independent of the external driving forces the internal dynamics also play a determining role through such things as the viscosity and the surface tension of the particular material. These results suggest the transient heat flow and resulting vapor film growth affect the interaction of the hot material and the coolant in a way that only a detailed calculation can make clear. A complete model should include both the

hydrodynamic and thermal effects. However, the second point mentioned earlier suggest there are domains in which thermal effects are dominant.

Kazimi[3] has developed a model of vapor film growth which starts from a gaseous (non-condensable) film ($<10^{-15}$ cm thick) surrounding a molten sphere at the time of contact. The subsequent heat flow is used to calculate the rate of vaporization according to the equation

$$L \frac{dm_v}{dt} = -k_H \frac{\partial T_H}{\partial r}\bigg|_R + k_\ell \frac{\partial T_\ell}{\partial r}\bigg|_{R_\delta} \qquad (1.1)$$

where L is the heat of vaporization, m_v is the mass of vapor, k_H is the thermal conductivity of the hot body, k_ℓ is the thermal conductivity of the liquid coolant, T_H is the temperature of the hot body and T_ℓ is the temperature of the coolant. We note parenthetically that there is some question of the validity of equation (1.1) in the particular circumstances but defer discussion of this point to Chapter IV. This vapor then expands as its temperature rises but because of inertia it over expands causing a pressure drop. Then as the vapor contracts, there is more heat flow and more vaporization so that a forced oscillation is setup which eventually dies out as the temperature of the molten sphere approaches the temperature of the coolant.

There are three main results of this model.

a) Effect of Water Temperature

The oscillatory behavior is damped quickly when the water subcooling is small, in spite of the initially larger pulse. Higher vaporization rates are obtained at smaller values of water subcooling. This allows the film to grow smoothly without oscillations. The heat consumed in vaporization is found to be a small fraction of the total transferred heat in the model.

Experimentally, the fragmentation of different materials, including tin, have been observed to be enhanced with larger subcoolings of water and to be virtually non-existent when the water temperature is above 70°C.[4] One of the aims of this thesis is to establish the relationship between the interior pressure time history and the degree of subcooling of the water as given by this model.

b) Effect of the Hot Sphere Temperature

Pressure histories for the film around molten tin spheres initially at 400°C, 500°C and 700°C for the same water temperature, 20°C, have been calculated. The pressure oscillations are more vigorous initially (up to .5 msec) as the temperature is increased. The pressure oscillations are damped faster however for the sphere at 700°C initial temperature.

In Chapter III of this thesis we will give formulas for the internal pressures in the molten drop obtained

from assuming a driving pressure at the surface. At this point, it is enough to know that the solution for the internal pressure, $p(r,t)$ is

$$p(r,t) \sim \int_0^\infty \frac{p_\omega(a,t)e^{-i\omega t}}{\sin(ka)}\, d\omega \qquad (2)$$

where $k = \omega/C$

neglecting viscous and compressibility effects. Thus, if the Fourier component of $p(a,t) = p_\omega(a,t)$ is appreciable where $ka \sim \pi$, then large internal pressures both positive and negative can be obtained. One can see, then, that as the hot drop's temperature is increased the initial pressure increase becomes larger and sharper (in time) yielding a higher frequency so that k increases. Therefore as the term ka approaches π the internal pressures get larger. Of course, physically there are viscosity and compressibility effects so that the integral in Eq. (2) does not go to infinity but instead goes through a maximum and then diminishes. The experimental results of Cho[4] suggest an enhanced fragmentation for tin up to 500°C followed by a marked decrease in the fragmentation. Limited results of Witte, et al.[5] indicate an increase of fragmentation with temperature up to 700°C. Some British results indicate an increased fragmentation with temperature but also without an observed decrease for the temperature range investigated. We have not yet been able to analyze all these experiments sufficiently to resolve the apparent discrepancies in observed behavior.

CHAPTER II

THE ACOUSTIC WAVE IN A VISCOUS COMPRESSIBLE FLUID

CHAPTER II

THE ACOUSTIC WAVE IN A VISCOUS COMPRESSIBLE FLUID

In this chapter, we begin by deriving the wave equation for the pressure in a fluid.

The equation of continuity is

$$\frac{\partial \delta}{\partial t} + \rho \nabla \cdot \bar{u} = 0 \tag{2.1}$$

$\bar{u}$ is the velocity of the fluid at a point

δ is the small time varying part of the density

ρ is the equilibrium value of the density

and is a constant in space and time

D is the total density

or

$$D = \rho + \delta \tag{2.2}$$

and the first-order Stokes-Navier equation [6] is

$$\rho \frac{\partial \bar{u}}{\partial t} = - \nabla p + (\eta + 4/3\mu) \nabla (\nabla \cdot \bar{u}) - \mu \nabla \times (\nabla \times \bar{u}) \tag{2.3}$$

It is a fundamental theorem of vector calculus that any vector function of position such as $\bar{u}$ can always be uniquely separated into a longitudinal part $\bar{u}_l$ for which $\nabla \times \bar{u}_l = 0$ and a transverse part for which $\nabla \cdot \bar{u}_t = 0$.

So define

$$\nabla \times \bar{u}_\ell = 0 \tag{2.4}$$

$$\nabla \cdot \bar{u}_t = 0 \tag{2.5}$$

Thus substituting $\bar{u}_\ell$ and $\bar{u}_t$ into (2.3) separately and using (2.4 and 2.5) we obtain

$$\rho \frac{\partial \bar{u}_\ell}{\partial t} = - \nabla p + (\eta + 4/3\mu) \nabla^2 \bar{u}_\ell \tag{2.6}$$

$$\rho \frac{\partial \bar{u}_t}{\partial t} = - \mu \nabla \times (\nabla \times \bar{u}_t) \tag{2.7}$$

It must also be kept in mind that the gradient of a scalar function (in this case p) is entirely longitudinal, ie. since $\nabla \times \nabla p = 0$ for any p, the equation can be split into these two separate equations. Thus the transverse part of $\bar{u}$, $\bar{u}_t$ is unrelated to the pressure wave. The two parts of the velocity solution, $\bar{u}_\ell$ and $\bar{u}_t$ can be solved for separately and need not be combined until we come to satisfying the boundary conditions.

The continuity equation (3.1) can be rewritten as

$$\frac{\partial \delta}{\partial t} + \rho \nabla \cdot \bar{u}_\ell = 0, \text{ since } \nabla \cdot \bar{u}_t = 0 \tag{2.8}$$

Next, taking the time derivative of (2.8) we get

$$\frac{\partial^2 \delta}{\partial t^2} + \rho \nabla \cdot \frac{\partial \bar{u}_\ell}{\partial t} = 0 \qquad (2.9)$$

since

$$\frac{\partial \rho}{\partial t} = 0$$

Taking the gradient of (2.8) gives

$$\nabla \frac{\partial \delta}{\partial t} + \rho \nabla^2 u_\ell = 0 \qquad (2.10)$$

Using (2.10) to eliminate $\nabla^2 u_\ell$ in (2.6) gives

$$\rho \frac{\partial \bar{u}_\ell}{\partial t} = - \nabla p - (\eta + 4/3\mu) \frac{1}{\rho} \nabla \frac{\partial \delta}{\partial t} \qquad (2.11)$$

Taking the divergence of (2.11) gives

$$\rho \frac{\partial}{\partial t} \nabla \cdot \bar{u}_\ell = - \nabla^2 p - \frac{(\eta + 4/3\mu)}{\rho} \frac{\partial}{\partial t} \nabla^2 \delta \qquad (2.12)$$

Using (2.9) to replace the L.H.S. of (2.12) gives

$$\frac{\partial^2 \delta}{\partial t} = \nabla^2 p + \frac{(\eta + 4/3\mu)}{\rho} \frac{\partial}{\partial t} \nabla^2 \delta \qquad (2.13)$$

The next equation is the equation of continuity for heat flow.

$$T \frac{\partial \delta}{\partial t} = K \nabla^2 \tau \qquad (2.14)$$

where τ is the small time varying part of the temperature, T is the time independent equilibrium value of the temperature, and σ is the small time varying part of the entropy. We have omitted the viscosity loss term because it is second order in $\bar{u}$. The first order effects of viscosity enter in equation (2.12). The last two relationship needed are the equation of state, relating pressure, volume and temperature in the gas and the second law of thermodynamics, relating the entropy content of the fluid to the other variables. These equations are:

$$\delta = \left(\frac{\partial \rho}{\partial P}\right)_T p + \left(\frac{\partial \rho}{\partial T}\right)_P \tau \tag{2.15}$$

$$\sigma = \left(\frac{\partial S}{\partial T}\right)_p \tau + \left(\frac{\partial S}{\partial P}\right)_T p \tag{2.16}$$

where

$$K_T = -\frac{1}{V}\left(\frac{\partial V}{\partial P}\right)_T = \frac{1}{\rho}\left(\frac{\partial \rho}{\partial P}\right)_T \tag{2.17}$$

$$\beta = \frac{1}{V}\left(\frac{\partial V}{\partial T}\right)_P = -\frac{1}{\rho}\left(\frac{\partial \rho}{\partial T}\right)_P \tag{2.18}$$

Using (2.17) and (2.18) in (2.15) we obtain

$$\delta = \rho K_T p - \rho\beta\tau \tag{2.19}$$

and furthermore

$$C_V K_T = C_p K_S \text{ or } K_T = \gamma K_S \tag{2.20}$$

and

$$\alpha \equiv \left(\frac{\partial P}{\partial T}\right)_V = \beta / K_T \tag{2.21}$$

So using (2.20) and (2.21) in (2.19) we get

$$\delta = \rho K_T \ (p - \alpha\tau)$$

or

$$\delta = \rho\gamma K_S \ (p - \alpha\tau) \tag{2.22}$$

where

$$K_S \equiv -\frac{1}{V}\left(\frac{\partial V}{\partial P}\right)_S = \frac{1}{\rho}\left(\frac{\partial \rho}{\partial P}\right)_S$$

This result holds for any pure material for p and τ small compared to P and T. By similar methods we can obtain a similar equation for the entropy

$$\sigma = \frac{C_p}{T}\left(\tau - \frac{\gamma-1}{\alpha\gamma} p\right) \tag{2.23}$$

If we define

$$\ell_n = \frac{K}{\rho C_p C} \tag{2.24}$$

and use 2.24 and 2.23 in 2.14 we get

$$\ell_n \nabla^2 \tau = \frac{\partial}{\partial t}\left(\tau - \frac{\gamma-1}{\gamma\alpha}\right) p \tag{2.25}$$

Finally if we define

$$\ell_v = \frac{\eta + 4/3\mu}{\rho C} \tag{2.26}$$

and

$$C^2 = \frac{1}{\rho K_S} \tag{2.27}$$

then using (2.26) and (2.27) in (2.12) we get

$$\nabla^2 p = \frac{\gamma}{C^2}\left(\frac{\partial^2}{\partial t^2} - \ell v\, C\, \frac{\partial}{\partial t}\nabla^2\right)(p - \alpha\tau) \tag{2.28}$$

Equation (2.28) is the wave equation, modified for the effects of viscosity and thermal conduction. If there were no conduction, ℓ_n would be zero (see 2.24), τ would have to equal to $(\gamma-1)\, p/\gamma\alpha$ and $\gamma(p-\alpha\tau)$ would equal p. This is the approximation which has been chosen. This corresponds to adiabatic wave motion and is a reasonable approximation for the times over which the phenomena of fragmentation occurs (10^{-8} to 10^{-4} seconds). However, in general there are two kinds of waves depending on which flow predominates. One of them (the adiabatic wave) has already been discussed. The other wave corresponds chiefly to heat diffusion; here p is small compared with $\alpha\tau$, and the wave velocity is proportional to i indicating rapid attenuation. This means that this mode is important only near the boundaries.

Thus except for fluids with high viscosity or conductivity, (2.28) with $\gamma(p-\alpha\tau) = p$ will adequately describe the acoustic behaviour of the medium everywhere outside a small boundary layer. A more careful examination of the problem would include the simultaneous solution of (2.28) and (2.25).

Finally we put (2.28) in the form used

$$\nabla^2 p = \frac{1}{C^2}\left(\frac{\partial^2}{\partial t} - \ell_v C \frac{\partial}{\partial t}\nabla^2\right) p \qquad (2.29)$$

Introducing the F. T. (Fourier Transform) of p or p_ω we obtain

$$(\nabla^2 + \frac{i\omega}{C}\nabla^2)\, p_\omega + k^2 p_\omega = 0 \qquad (2.30)$$

or

$$\nabla^2 p_\omega + \left[k^2/(1 + i\ell_v k)\right] p_\omega = 0 \qquad (2.31)$$

or

$$\nabla^2 p_\omega + K^2 p_\omega = 0 \qquad (2.32)$$

where

$$K^2 = \frac{k^2(1 - i\ell_v k)}{(1 + \ell_v^2 k^2)} \quad \text{and} \quad k^2 = \frac{\omega^2}{C^2}$$

The result then of viscosity is to make the wave number complex indicating attenuation of the wave. This result, (2.32) will be used in Chapter III. It has two approximations inherent in its use. First it is a small amplitude approximation and second it

is for an adiabatic wave. We have calculated ℓ_v for tin at 500°C and found $\ell_v = 3.1 \times 10^{-7}$ which shows that the attenuation due to viscosity effects is quite small so that losses due to transmission at the boundary is probably the dominant energy loss mechanism.

CHAPTER III

THE ACOUSTIC WAVE NEGLECTING VISCOSITY

CHAPTER III

THE ACOUSTIC WAVE NEGLECTING VISCOSITY

In Chapter I we discussed the results of a model by Kazimi[3] in which vapor film growth at the surface of a hot liquid sphere (usually metallic) gives rise to a pressurization in time of the surface of the hot globule. In this chapter we will develop the equations for the interior and exterior pressure wave as a function of space and time and will present the numerical results of these equations for various of the cases for which the pressure wave at the surface is already known.

III.1 Theoretical Results

We begin by taking the wave equation developed in Chapter II (equation 2.29) as our starting point. This equation was derived in the small amplitude approximation for the general case of a viscous fluid with thermal conduction. We begin by neglecting viscous effects, that is taking $\ell_v = 0$ so

$$\nabla^2 p - \frac{1}{C^2} \frac{\partial^2 p}{\partial t^2} = f(\bar{r},t) \text{ where } C^2 = \frac{1}{\rho K_s} \qquad (3.1)$$

where $f(\bar{r},t)$ is the volumetric driving pressure (or inhomogenous term), ρ is the density of the medium, K_s is the isentropic compressibility, C is the speed of sound, and p is the pressure difference from equilibrium at a point.

We apply the Fourier transform (F.T.) technique which gives

$$p(\bar{r},t) = \int_{-\infty}^{\infty} p_\omega e^{-i\omega t}\, d\omega \tag{3.2}$$

and

$$p_\omega(\bar{r}) = \frac{1}{2\pi} \int_{-\infty}^{\infty} p(\bar{r},t)\, e^{+i\omega t}\, dt \tag{3.3}$$

where p_ω is the F.T. of p.

The F. T. of equation (3.1) is

$$\nabla^2 p_\omega + k^2 p_\omega = - f_\omega(\bar{r}) \tag{3.4}$$

where

$$f_\omega = \frac{1}{2\pi} \int_{-\infty}^{\infty} f(\bar{r},t)\, e^{+i\omega t}\, dt \tag{3.5}$$

and

$$k^2 \equiv \omega^2/c^2 \tag{3.6}$$

Define g_ω such that

$$\nabla^2 g_\omega(\bar{r},\bar{r}_o) + k^2 g_\omega(\bar{r},\bar{r}_o) = - \delta(\bar{r},\bar{r}_o) \tag{3.7}$$

This g_ω is the F.T. of the Green's function for an infinite medium. However, to satisfy the boundary conditions which necessarily include reflections at the wall we add χ.

Where

$$\nabla^2\chi + k^2\chi = 0 \tag{3.8}$$

So the F.T. of the appropriate Greens function for the problem is defined by

$$G_\omega(\bar{r},\bar{r}_o) = g_\omega(\bar{r},\bar{r}_o) + \chi \tag{3.9}$$

Next using one of Green's theorems

$$p_\omega = \int_{V_o} f_\omega\, G_\omega\, dV_o + \int_{S_o} [G_\omega \frac{\partial}{\partial n_o} p_\omega - p_\omega(r_o) \frac{\partial}{\partial n_o} G_\omega]\, dS_o \tag{3.10}$$

where n_o is the outward pointing normal and $\frac{\partial}{\partial n_o}$ is the normal derivative at the surface.

In the case at hand we believe that the dominant source of radiation is the pulsating surface of the sphere. So for the purposes of the model it should be sufficient to consider only the surface terms and this is of course a convenient simplification. For these reasons, we set $f_\omega = 0$. We then obtain

$$p_\omega = \int_{S_o} [G_\omega \frac{\partial}{\partial n_o} p_\omega - p_\omega \frac{\partial}{\partial n_o} G_\omega]\, ds. \tag{3.12}$$

($r = r_o = a$ defines S_o in this case)

It is clear then, that p_ω can be calculated in general if we know $p_\omega(a)$ and $\frac{\partial}{\partial n_o} p_\omega(a)$. However we can make another simplifying assumption which should give the right trends to the pressure although it is not a particularly good assumption. The assumption we introduce is the assumption of rigid boundaries which has the result that $G_\omega(a) = 0$. Using this result gives

$$p_\omega(\bar{r}) = - \int_{S_o} p_\omega(a) \frac{\partial}{\partial n_o} G_\omega(\bar{r},\bar{r}_o)\, ds. \tag{3.13}$$

Now the Green's function for an infinite medium is

$$g_\omega = \frac{ik}{4\pi} h_o(kR) \tag{3.14}$$

h_o is a zero order spherical Hankel function and

$$R = |\bar{r}-\bar{r}_o|$$

The expansion of g_ω in spherical coordinates in terms of the coordinates r, θ, ϕ of the measurement point and r_o, θ_o, ϕ_o of the source point is

$$g_\omega = \frac{ik}{4\pi} \sum_{m,n,o} (2m+1)\, \epsilon_n \frac{(m-n)!}{(m+n)!} \chi \tag{3.15}$$

$$\times Y^G_{m,n}(\theta,\phi) Y^G_{m,n}(\theta_o,\phi_o) \begin{cases} j_m(kr_o) h_m(kr) & r > r_o \\ j_m(kr) h_m(kr_o) & r < r_o \end{cases}$$

$$r, r_o \leq a$$

and G_ω is found as

$$G_\omega = \frac{ik}{4\pi} \sum_{m=0} (2m+1) \sum_{n,\sigma} \varepsilon_n \frac{(m-n)!}{(m+n)!} Y^G_{m,n}(\theta_o,\phi_o)$$

$$\times [H_m - A j_m(kr) j_m(kr)] \qquad (3.16)$$

Imposing the condition that $G_\omega = 0$ at $r_o = a$ gives

$$j_m(kr) h_m(kc) - A j_m(kr)\ j_m(ka) = 0 \qquad (3.17)$$

or

$$A = \frac{h_m(ka)}{j_m(ka)} \qquad (3.18)$$

We need $\frac{\partial}{\partial n_o} G_\omega$ which we can now calculate as

$$\frac{\partial G_\omega}{\partial n_o}\bigg|_{r_o=a} = \frac{ik}{4\pi} \sum_{m=0} (2m+1) \sum_{n,\sigma} \varepsilon_n \frac{(m-n)!}{(m+n)!} Y^\sigma_{m,n}(\theta,\phi)$$

$$\times Y^\sigma_{m,n}(\theta_o,\phi_o) * \frac{\partial}{\partial n_o} [H_m - \frac{h_m(ka)}{j_m(ka)} j_m(kr) j_m(kr_o)]$$

$$r = a \qquad (3.19)$$

and after some algebra

$$\frac{\partial}{\partial n_o} [H_m - \frac{h_m(ka)}{j_m(ka)} j_m(kr) j_m(kr_o)]\ r_o = a \qquad (3.20)$$

$$= \frac{ik}{k^2 a^2} \frac{j_m(kr)}{j_m(ka)}$$

Using equation (3.20) in (3.19) and substituting for $\frac{\partial G_\omega}{\partial n_o}$ in equation (3.13) we obtain

$$p_\omega = \frac{1}{4\pi} \int_{4\pi} p_\omega(a) \sum_{m=0}^{\infty} \frac{j_m(kr)}{j_m(ka)} (2m+1) \sum_{n,\sigma} \varepsilon_n \frac{(m-n)!}{(m+n)!}$$

$$\times Y^{\sigma}_{m,n}(\theta,\phi)\, Y^{\sigma}_{m,n}(\theta_o,\phi_o)\, d\Omega_o \qquad (3.21)$$

Now

$$\int_{4\pi} Y^{\sigma}_{m,n}(\theta_o,\phi_o)\, d\Omega_o = 2\pi\, \delta m_o\, \delta n_o\, \delta\sigma_1 \qquad (3.22)$$

and

$$Y^{1}_{o,o} = Y_o = P_o = 1 \qquad (3.23)$$

This means that since there is no angular dependance in (3.23) we need only the zero order spherical harmonics which are also angle independent.

We get

$$p(r,t) = \int_{-\infty}^{\infty} \frac{jo(kr)}{j_o(ka)}\, p_\omega(a) e^{-i\omega t}\, d\omega \qquad (3.24)$$

where

$$j_o(z) = (\sin z)/z \text{ and } k = \omega/C$$

So, using equation (3.24)

$$p(r,t) = \int_{-\infty}^{\infty} \frac{a}{r} \frac{\sin kr}{\sin ka}\, p_\omega(a)\, e^{-i\omega t}\, d\omega \qquad (3.25)$$

It is also useful to have an explicit expression for $p(r = o,t)$ which is

$$p(r = o,t) = \int_{-\infty}^{\infty} \frac{ka}{\sin ka}\, p_\omega(a)\, e^{-i\omega t}\, d\omega \qquad (3.26)$$

Furthermore we need the limiting forms for the multiplying factors of $p_\omega(a)$ in equation (3.25) and (3.26)

So

$$\lim_{k\to o} \frac{a}{r} \frac{\sin kr}{\sin ka} = 1 \qquad (3.27)$$

and

$$\lim_{k\to o} \frac{ka}{\sin ka} = 1 \qquad (3.28)$$

We are now in a position to calculate the interior pressure wave given the pressure at the surface. Numerically this is accomplished by the use of the Fast Fourier Transform (FFT) method due to Cooley and Tukey[7]. This method has been implemented by Norman Brenner[8] of the MIT Department of Earth and Planetary Sciences and is on the Math Library Tape as a load module in single precision. It is called FOURT. This program is used as a Fortran subroutine to calculate both the forward and inverse transform.

The solution p(r,t) expressed in equation (3.25) has some practical limitations besides the ones imposed by the various assumptions which have been made. The most important limitation is that as the wavelength corresponding to the frequency at which p_ω is small compared to p_ω at $\omega = o$ becomes much smaller than the radius of the sphere, the solution has many peaks and valleys which require a large number of

mesh points over which $p(a,t)$ and $p_\omega(a)$ must be known. Further, more and more significant figures must be carried in order to get meaningful results. One measure of how good the results obtained are is how small the calculated imaginary part of $p(r,t)$ is. This is because both the real and imaginary parts satisfy the wave equation and the boundary condition for the imaginary part is that it be zero at time equal zero. In the results obtained to date, the imaginary part of $p(r,t)$ has been a factor of 10^5 smaller than the real part in all cases. This limitation can be alleviated to some extent by using FOURT in double precision but it can not be entirely eliminated.

The model so far presented also is limited by two assumptions which have been made. The first and least serious is the neglect of viscosity. This has the effect of making the absolute value of the pressure calculated in the model too large. Its neglect also leads to the singular behaviour of $p(r,t)$ as given in equation (3.25) since at $ka = \pi$ the integrand blows up. In Chapter II, we included viscosity effects and those results have led to the introduction of a convergence factor into equation (3.25) in the following way:

$$k = \omega/C - i\varepsilon$$

where ϵ is the convergence factor taken as .01 to avoid the previously mentioned singularity. Of course, since ϵ is so small, it has no practical effect except at $ka \approx \pi$. The second assumption of rigid walls is a poor approximation but can still serve as a point of departure. Neglect of transmission of the pressure wave is a large effect which also causes the calculated pressures to be too large in absolute value. The inclusion of this effect will be discussed in Chapter IV. Finally, the most important property of equation (3.25) is the resonance behaviour which it exhibits. That is, when $ka = n\pi$, the calculated pressures get very large (infinite if viscosity is neglected). This will lead to subatmospheric pressures (as we will see) and even negative pressures. A third limitation as was mentioned earlier is the small amplitude approximation, which means that $p/P \ll 1$ for the wave equation to hold. One must, therefore, keep in mind that strictly speaking these results are not applicable when $p \gtrsim P$. However, the calculated pressures are certainly indicative of the main trends within the limitations already mentioned.

III.1 Numerical Results

In this section the numerical results for various cases will be discussed. These cases will be the same

as some of those done by Kazimi[3]. They are given in Table 3.1 which shows that the variation of the radius has been divided into two parts. One part deals with the variation caused by varying the radius and not the pressure at the surface and the second part is concerned with the radius variation plus the corresponding change in the surface pressure. The first case which is of interest to investigate is the r-dependance.

I. Radial Dependance

For a small radius (a = .1cm), figure 3.1 shows a series of pressure versus time curves (all overlapping) for each of five radii (r = 0, a/5, 2a/5, 3a/5, 4a/5, a, a = .1 cm). In this figure, one can see that there is essentially no change. One can understand this result by taking the limit of equation (3.25) as a (and subsequently r, since $r \leq a$) goes to zero. The result of this limiting process is to show that the multiplicative factor of $p_\omega(a)$ goes to one which means that $p(r,t)$ approaches $p(a,t)$ for all r. This can be understood physically as a case in which the system will follow the driving function if the dimensions are small compared to the wavelengths present in the driving function, i.e. for a = .1 cm, $.3 \leq \lambda \leq 50$ cm.

TABLE 3.1

VARIABLES \ CASE NUMBER	1	2	3	4	5	9	10
Initial Sphere Temperature, °C	500	500	500	400	700	700	700
Water Pool Temperature, °C	20	50	80	20	20	20	20
Sphere Radius, cm	Varied	.3	.3	.3	.3	.1	1.0
Initial Film Thickness, cm	10^{-5}	10^{-5}	10^{-5}	10^{-5}	10^{-5}	10^{-5}	10^{-5}
Radius Corresponding to Assumed Driving Pressure,	.3	.3	.3	.3	.3	.1	1.0
Figure Showing Results	3.3-3.6 & 3.11	3.12	3.13	3.10	3.8	3.7	3.9

II. Effect of Radius (a) of Sphere

a) In figures 3.1, 3.2, 3.3, 3.4, 3.5 and 3.6 the pressure time history at r = 0 for case (1) for the different values of a = .1, .2, .3, .5, .75, 1.0 cm is shown. It can be seen that the absolute value of the pressure swings in the initial pulse (the transient behaviour) increases as a increases. However, the lower frequency oscillations that follow are relatively unaffected as the transient behaviour decays out. This is a resonance effect for the high frequencies such that $ka = \pi$. However for the rest of the pulse for the radii studied, conditions are off resonance. In this case (1) the driving function is kept the same for all radii and corresponds to the Kazimi calculated function for a = 0.3 cm.

b) Next the total effect of varying the radius is considered. This includes the variation in the surface pressure caused by varying the radius. These cases are labelled 9, 5, and 10 and the results are shown in figures 3.7, 3.8, and 3.9 for r = 0, a = .1, .3 and 1.0 cm. The trend here is also for the absolute value of the pressure in the transient to increase except that the variation is much more dramatic as a result of including the increases in the initial pulse. It should be kept in mind that the low frequency oscillations in the 10^{-5} to 10^{-3} sec time domain are relatively unaffected. The rise times of the

initial positive going part are getting longer in contrast to the experimental data of references 3 and 4. However, one can't make too much of the trend as the rise times in the experimental data are typically 100 - 500 micro-seconds whereas the Kazimi model gives approximately 1 micro-second. Furthermore, it seems clear that the pressure pulse being measured is the final pressurization of the explosion while the calculated pressures are those which preceed the explosion and possibly are causing the internal vaporization which leads to the explosion.

III. Effect of Hot Sphere Temperature

There is a body of evidence (reviewed in reference 3) which shows that fragmentation is more extensive as the hot body temperature is increased. Presumably this would mean the pressure down swings would be longer and deeper to induce this larger extent of fragmentation. This has been investigated in cases 4, 1, and 5 in this work. The results of the pressure calculation shown in figures 3.10, 3.3 and 3.8 for r = 0 and a = .3 cm was carried out at hot body temperatures of 400, 500 and 700°C. As temperature goes up, the amplitude of the transient (both plus and minus swings) gets larger. In all cases the pressure goes negative several times but for short periods (about 1 micro-second).

Furthermore, this is still too short a time to correspond to the experimental results although bubbles initiated at these times could grow in response to the subatmospheric part of the pulse which arrives later, if it were less than the vapor pressure of the hot liquid at that time and temperature.

IV. Effect of Water Temperature

Finally, the effect of increasing the temperature of the water was investigated for cases 1, 2 and 3 which corresponds to temperatures of 20, 50, and 80°C and the results for r = 0 are shown in figures 3.11, 3.12, and 3.13. Here can be seen that as the temperature increases the amplitude of the pressure swings also increases. This occurs because of the increase in the peak pressure at the surface in conjunction with a constant rise time. This effect is in marked contrast to the experimental data in which the fragmentation is less and less as the water temperature is increased. One is therefore tempted to believe that the fragmentation is best correlated with the amount of undershoot at the later times even though the undershoot never comes down below 5 psi which is still well above the vapor pressure of the hot liquid (which is in the range of 10 to 40 mm of Hg).

FIGURE 3.1

Pressure time history for Case 1
and r=0.0, .02, .04, .06, .08 and .1 cm, a=.1cm
and T_H=500°C

FIGURE 3.1

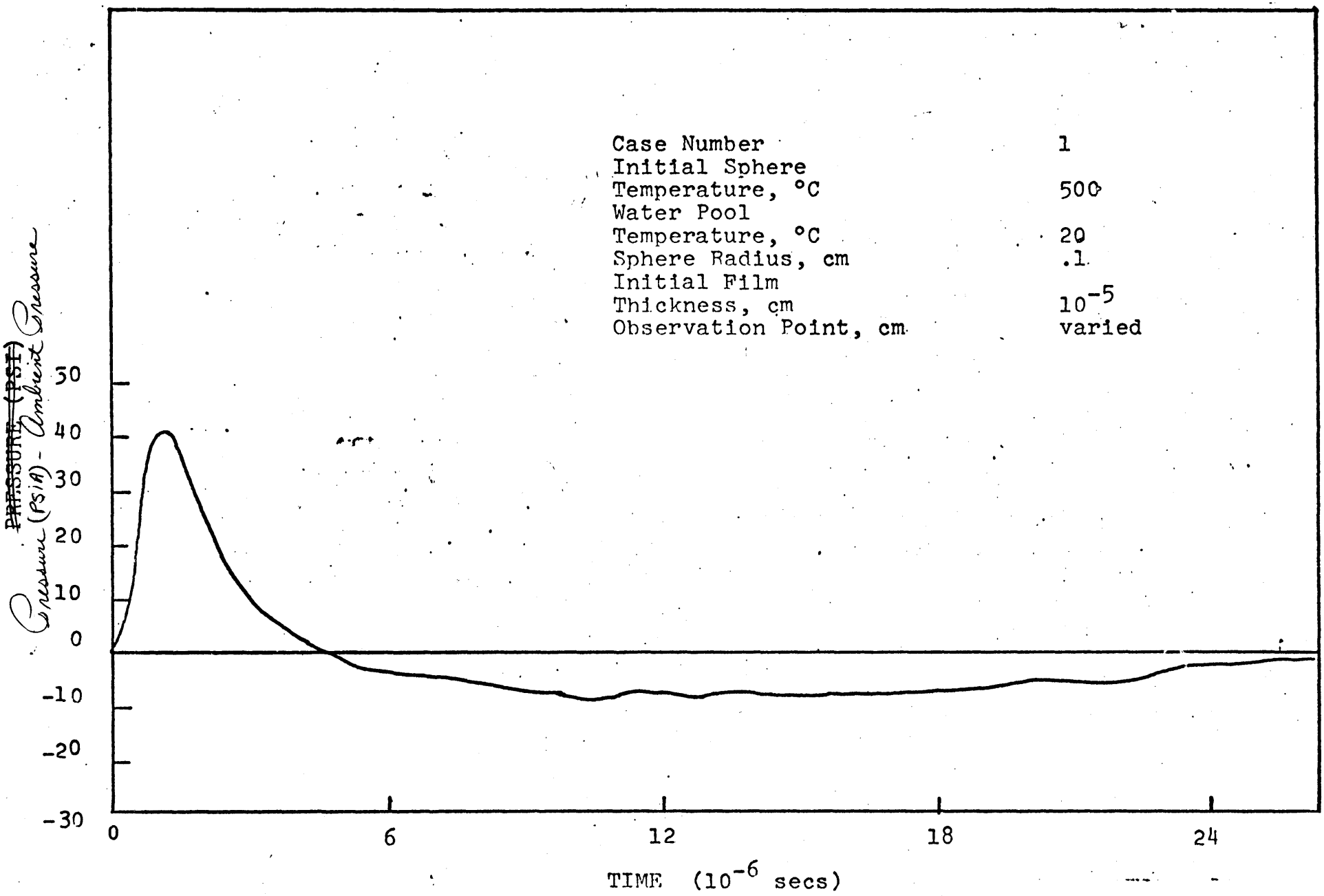
Case Number 1
Initial Sphere Temperature, °C 500
Water Pool Temperature, °C 20
Sphere Radius, cm .1
Initial Film Thickness, cm 10^{-5}
Observation Point, cm varied
PRESSURE (PSI)
Pressure (PSIA) - Ambient Pressure
50
40
30
20
10
0
-10
-20
-30
0
6
12
18
24
TIME (10^{-6} secs)

FIGURE 3.2

Pressure time history for Case 1
and r=0, a=.2cm

FIGURE 3.2

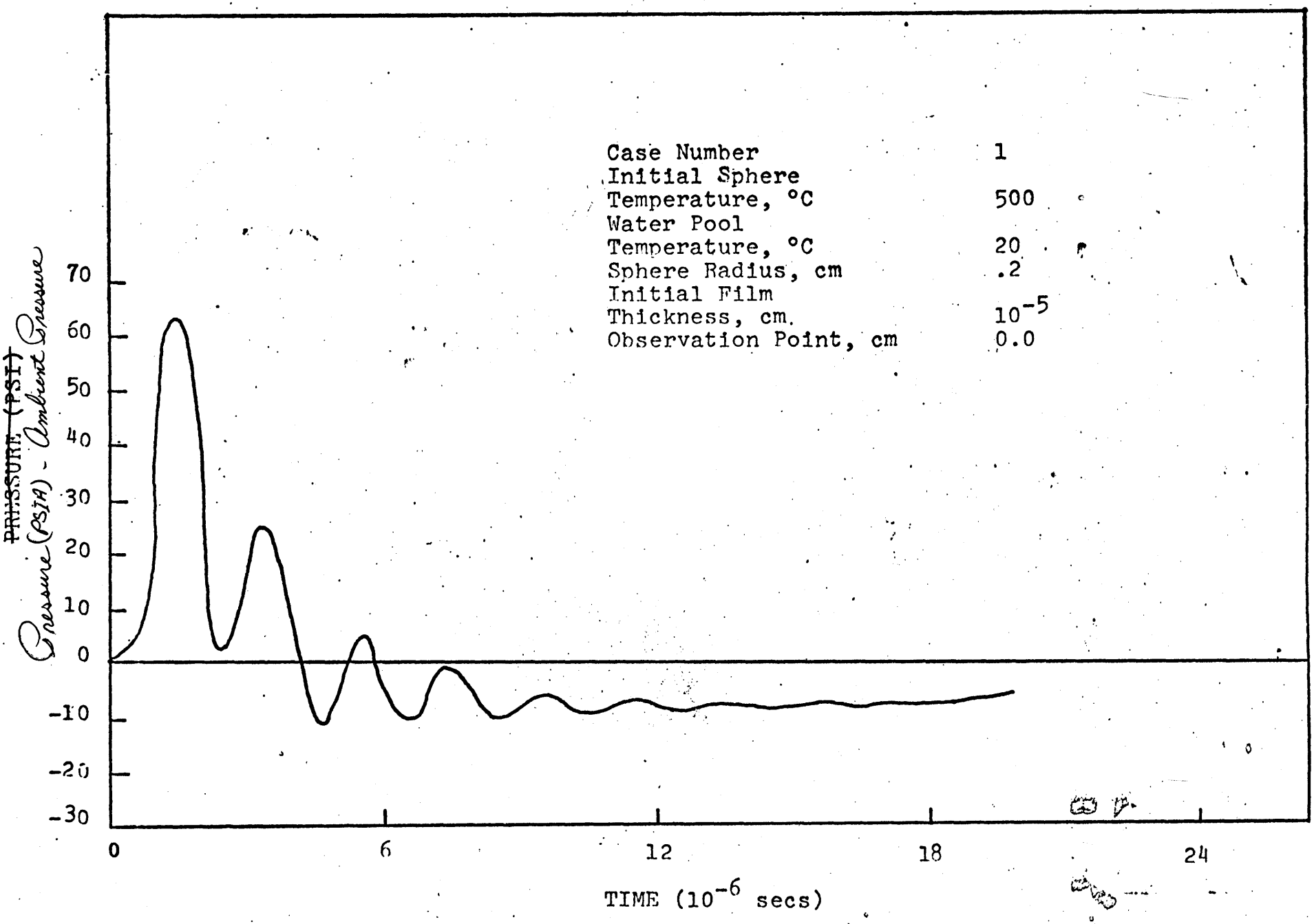
Case Number 1
Initial Sphere Temperature, °C 500
Water Pool Temperature, °C 20
Sphere Radius, cm .2
Initial Film Thickness, cm. 10^{-5}
Observation Point, cm 0.0
PRESSURE (PSI)
Pressure (PSIA) - Ambient Pressure
70
60
50
40
30
20
10
0
-10
-20
-30
0
6
12
18
24
TIME (10^{-6} secs)

FIGURE 3.3

Pressure time history for Case 1
and r=0, a=.3cm

FIGURE 3.3

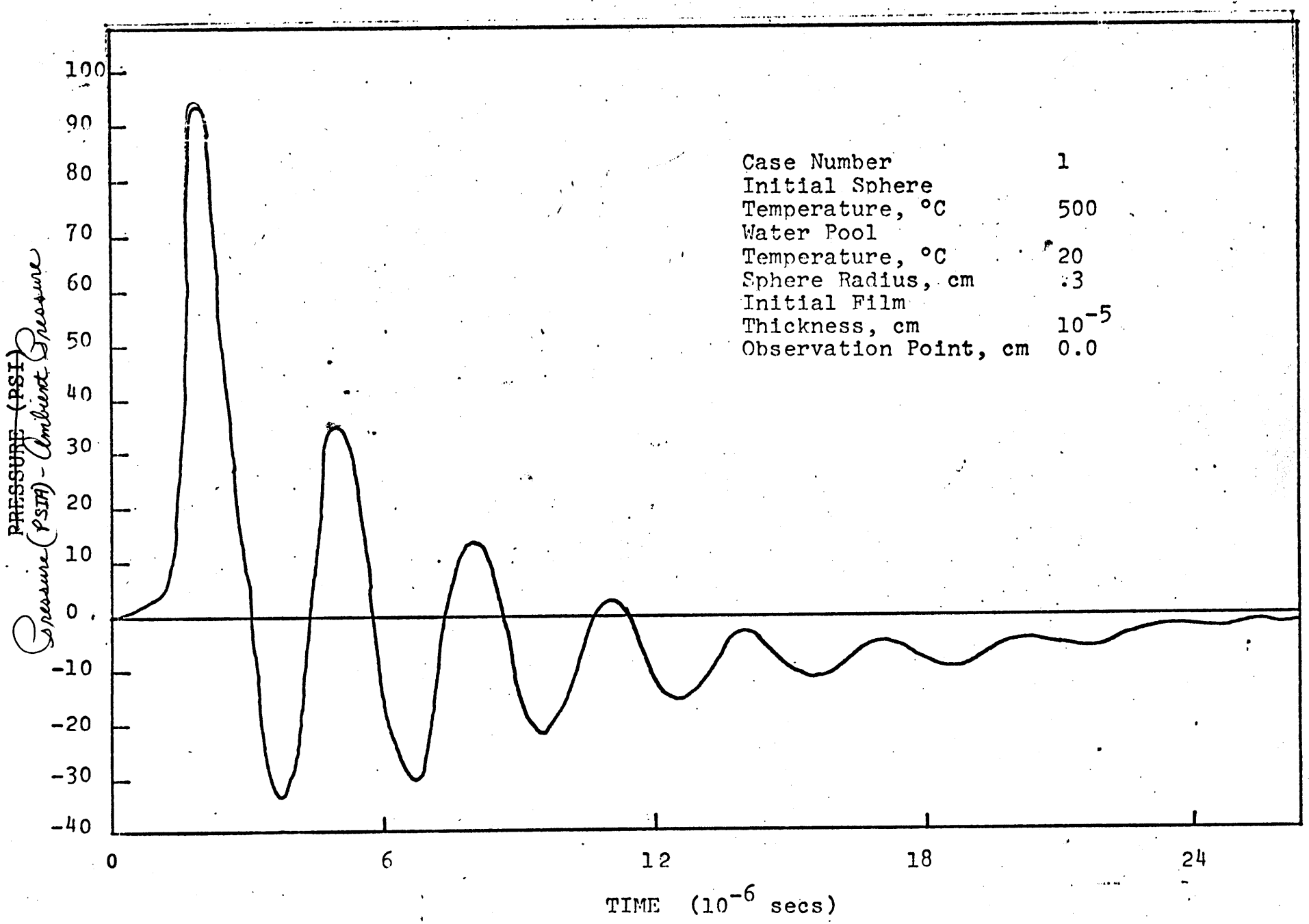
Case Number 1
Initial Sphere Temperature, °C 500
Water Pool Temperature, °C 20
Sphere Radius, cm .3
Initial Film Thickness, cm 10^{-5}
Observation Point, cm 0.0
PRESSURE (PSI)
Pressure (PSIA) - Ambient Pressure
100
90
80
70
60
50
40
30
20
10
0
-10
-20
-30
-40
0
6
12
18
24
TIME (10^{-6} secs)

FIGURE 3.4

Pressure time history for Case 1
and r=0, a=.5cm

FIGURE 3.4

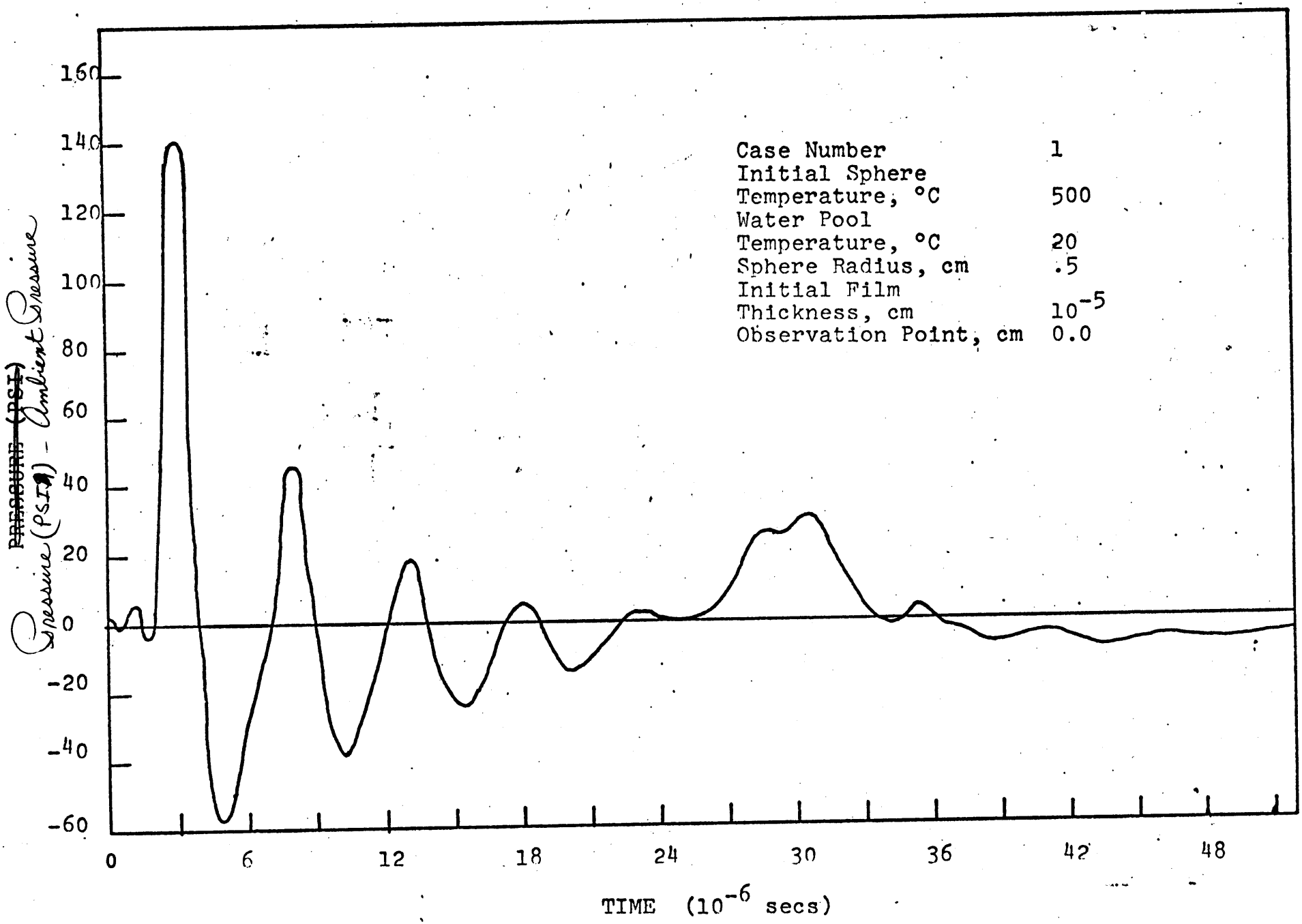
Case Number 1
Initial Sphere Temperature, °C 500
Water Pool Temperature, °C 20
Sphere Radius, cm .5
Initial Film Thickness, cm 10^{-5}
Observation Point, cm 0.0
PRESSURE (PSI)
Pressure (PSI) - Ambient Pressure
160
140
120
100
80
60
40
20
0
-20
-40
-60
0
6
12
18
24
30
36
42
48
TIME (10^{-6} secs)

FIGURE 3.5

Pressure time history for Case 1
and r=0, a=.75cm

FIGURE 3.5

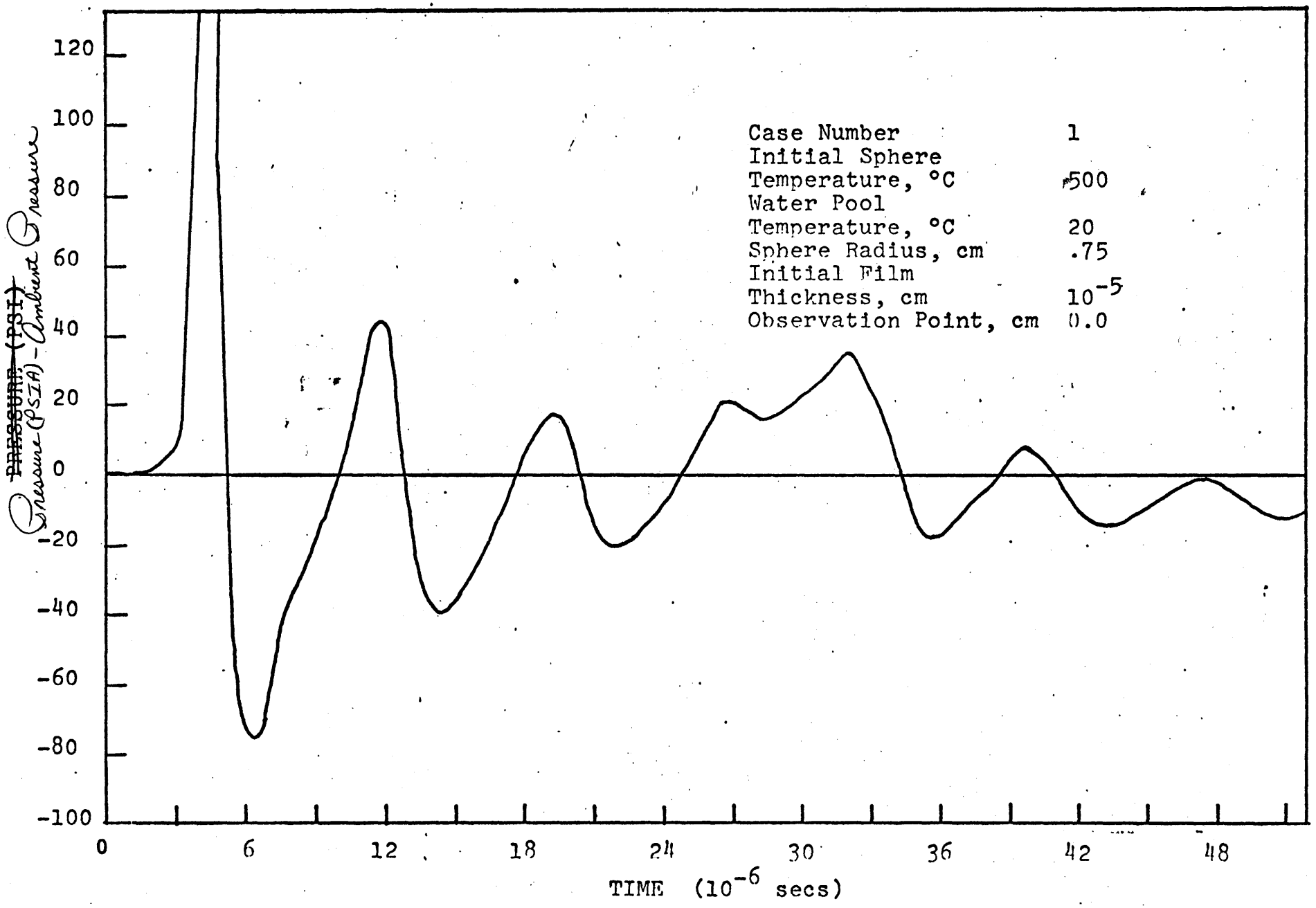
Case Number 1
Initial Sphere Temperature, °C 500
Water Pool Temperature, °C 20
Sphere Radius, cm .75
Initial Film Thickness, cm 10^{-5}
Observation Point, cm 0.0
Pressure (PSIA) - Ambient Pressure
120
100
80
60
40
20
0
-20
-40
-60
-80
-100
0
6
12
18
24
30
36
42
48
TIME (10^{-6} secs)

FIGURE 3.6

Pressure time history for Case 1
and r=0, a=1.0cm

FIGURE 3.6

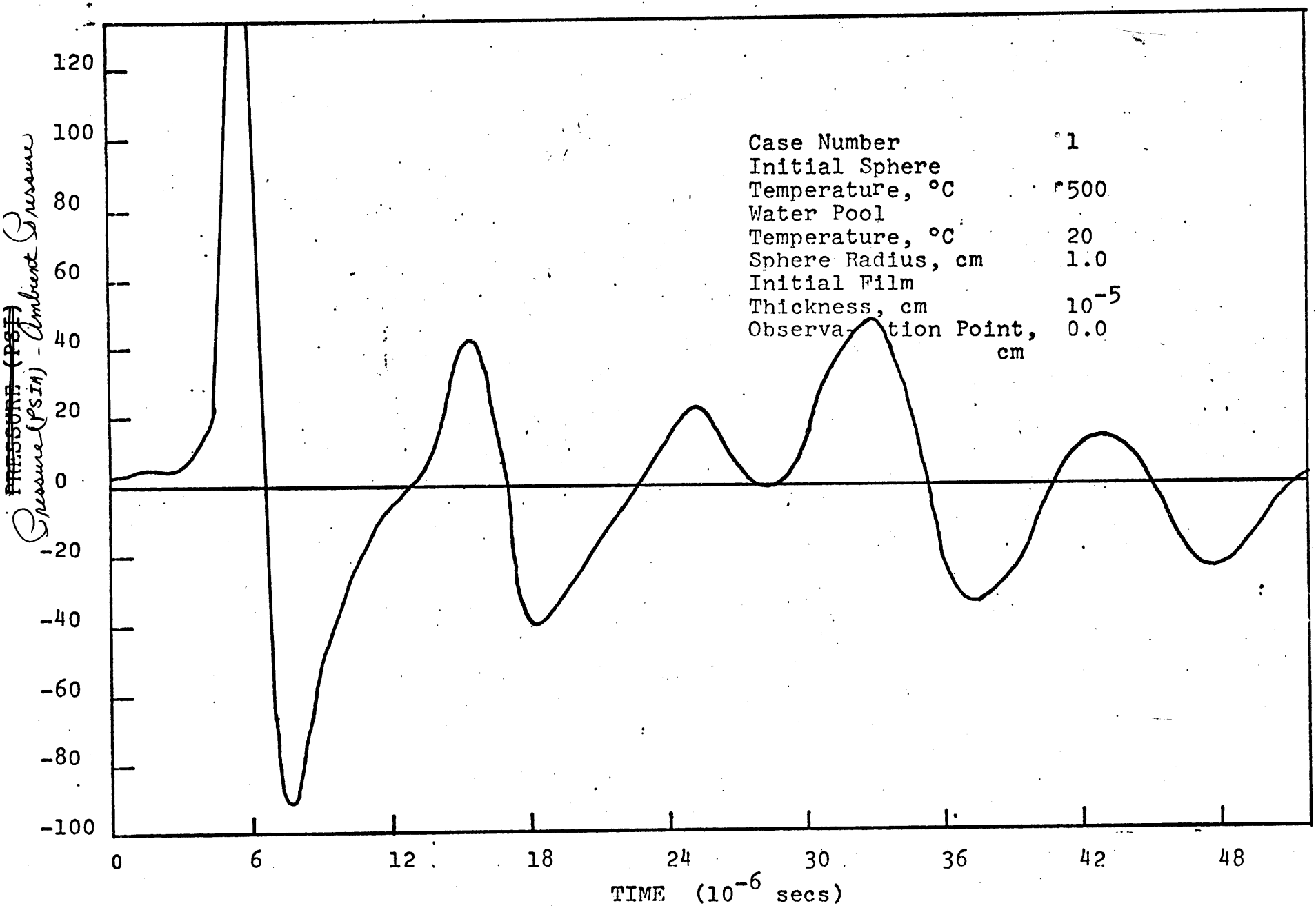
Case Number 1
Initial Sphere Temperature, °C 500
Water Pool Temperature, °C 20
Sphere Radius, cm 1.0
Initial Film Thickness, cm 10^{-5}
Observation Point, cm 0.0
Pressure (PSI) - Ambient Pressure
120
100
80
60
40
20
0
-20
-40
-60
-80
-100
0
6
12
18
24
30
36
42
48
TIME (10^{-6} secs)

FIGURE 3.7

Pressure time history for Case 9
r=0, and a=.1cm

FIGURE 3.7

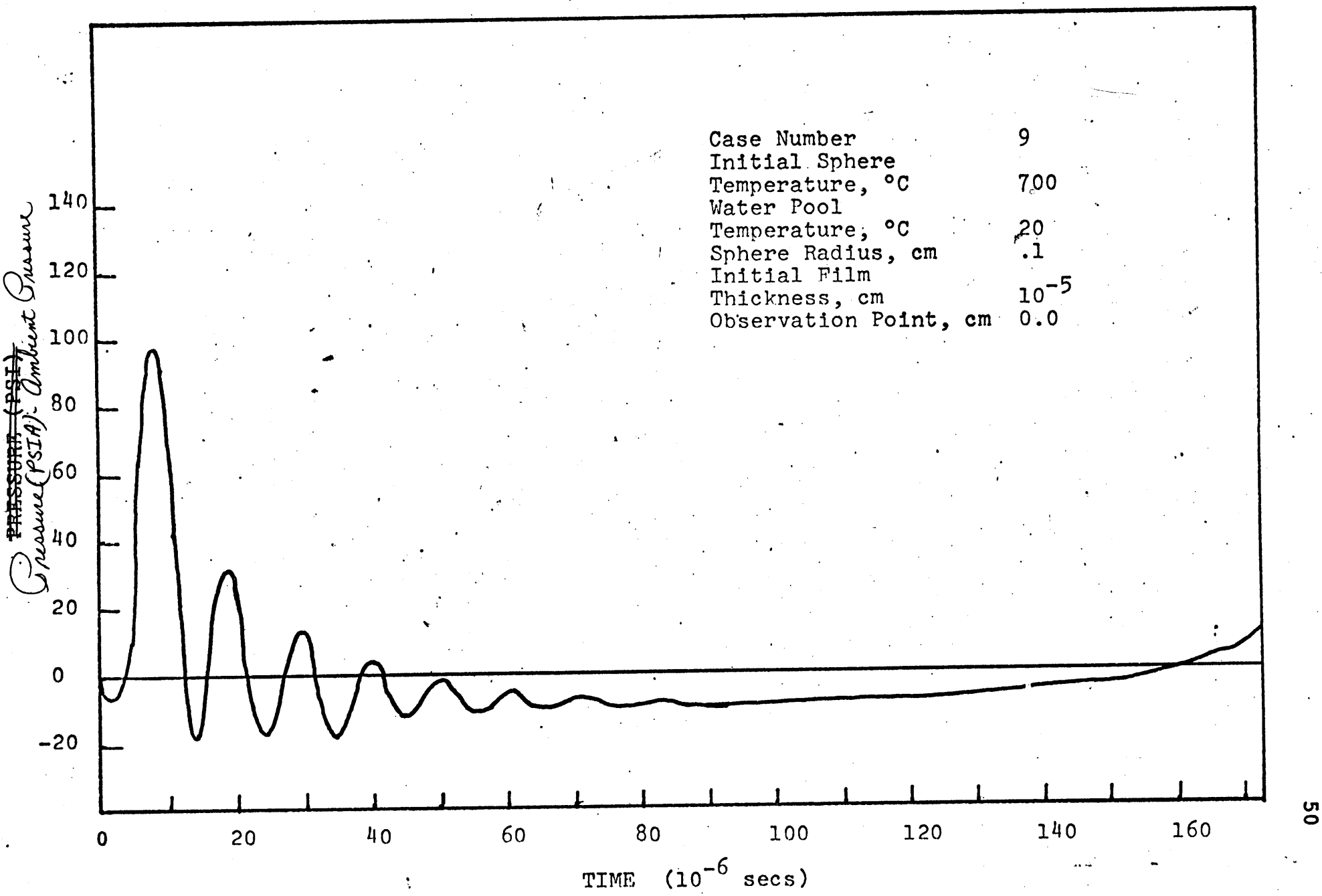
Case Number 9
Initial Sphere Temperature, °C 700
Water Pool Temperature, °C 20
Sphere Radius, cm .1
Initial Film Thickness, cm 10^{-5}
Observation Point, cm 0.0
PRESSURE (PSI)
Pressure (PSIA) - Ambient Pressure
140
120
100
80
60
40
20
0
-20
0
20
40
60
80
100
120
140
160
TIME (10^{-6} secs)

FIGURE 3.8

Pressure time history for Case 5
r=0 and a=.3cm
T_H=700°C

FIGURE 3.8

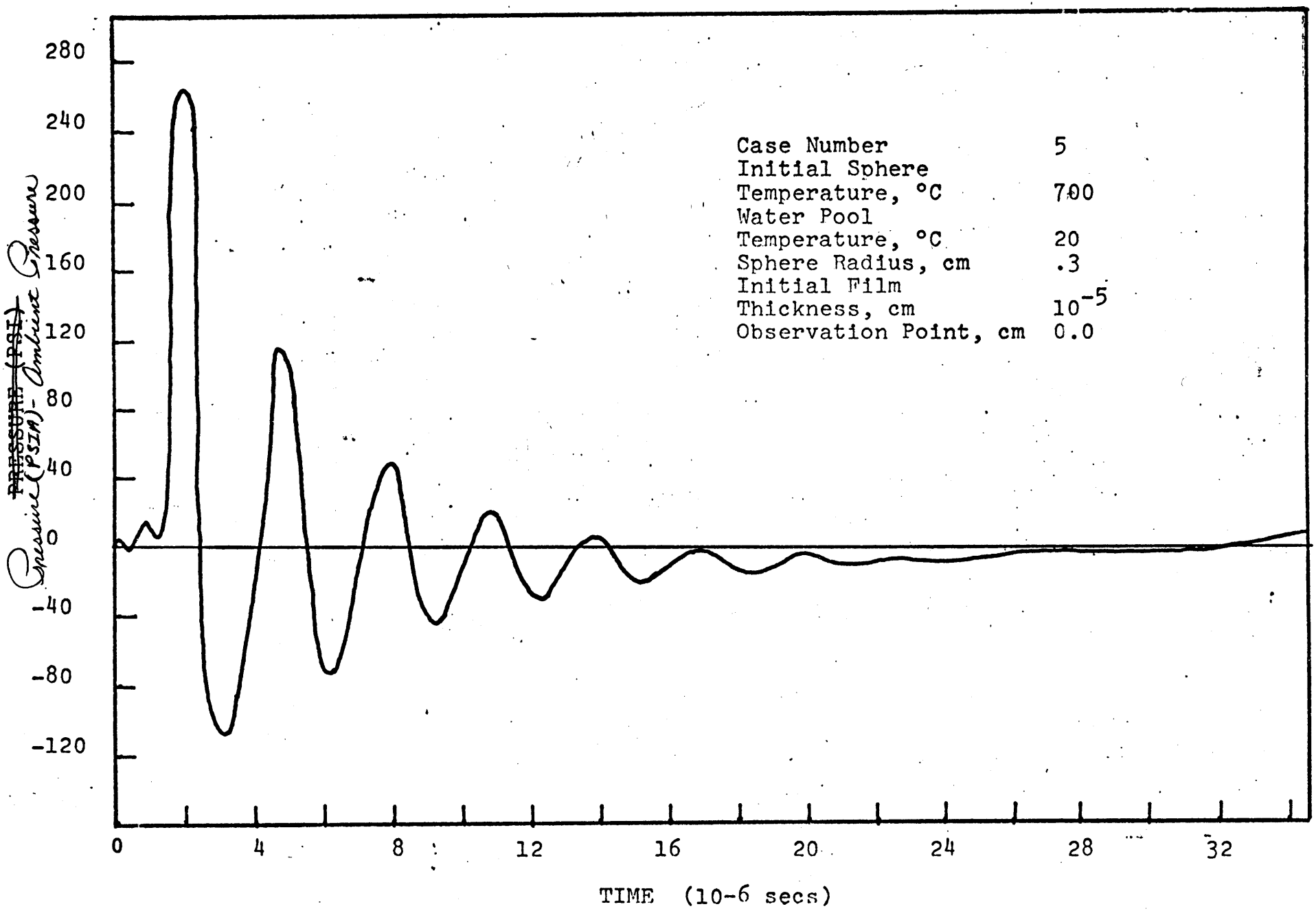
Case Number 5
Initial Sphere Temperature, °C 700
Water Pool Temperature, °C 20
Sphere Radius, cm .3
Initial Film Thickness, cm 10^{-5}
Observation Point, cm 0.0
PRESSURE (PSI)
Pressure (PSIA) - Ambient Pressure
280
240
200
160
120
80
40
0
-40
-80
-120
0
4
8
12
16
20
24
28
32
TIME (10-6 secs)

FIGURE 3.9

Pressure time history for Case 10
r=0 and a=1.0cm

FIGURE 3.9

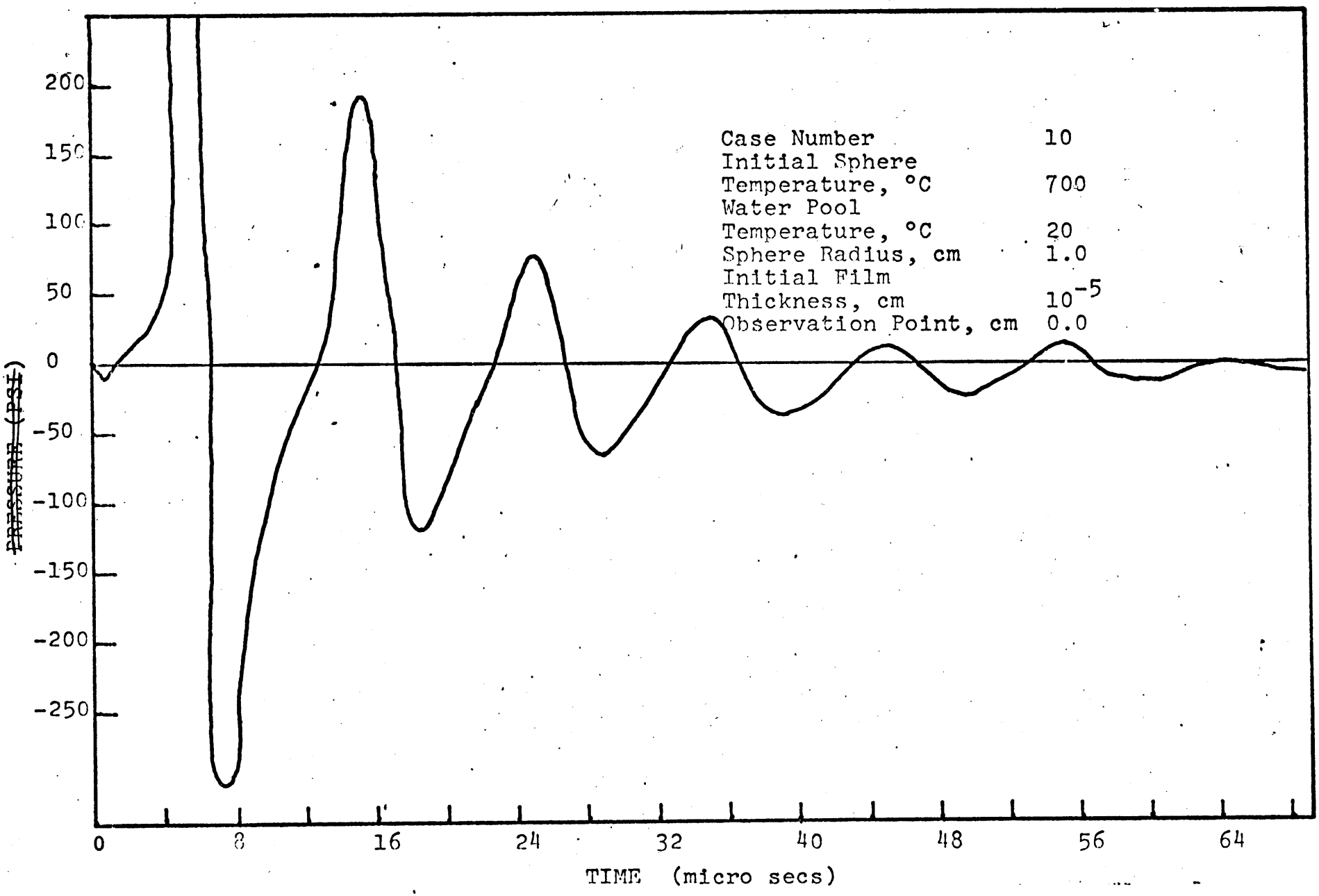
200
150
100
50
0
-50
-100
-150
-200
-250
PRESSURE (PSI)
0
8
16
24
32
40
48
56
64
TIME (micro secs)
Case Number 10
Initial Sphere Temperature, °C 700
Water Pool Temperature, °C 20
Sphere Radius, cm 1.0
Initial Film Thickness, cm 10^{-5}
Observation Point, cm 0.0

FIGURE 3.10

Pressure time history for Case 4
T_H=700°C

FIGURE 3.10

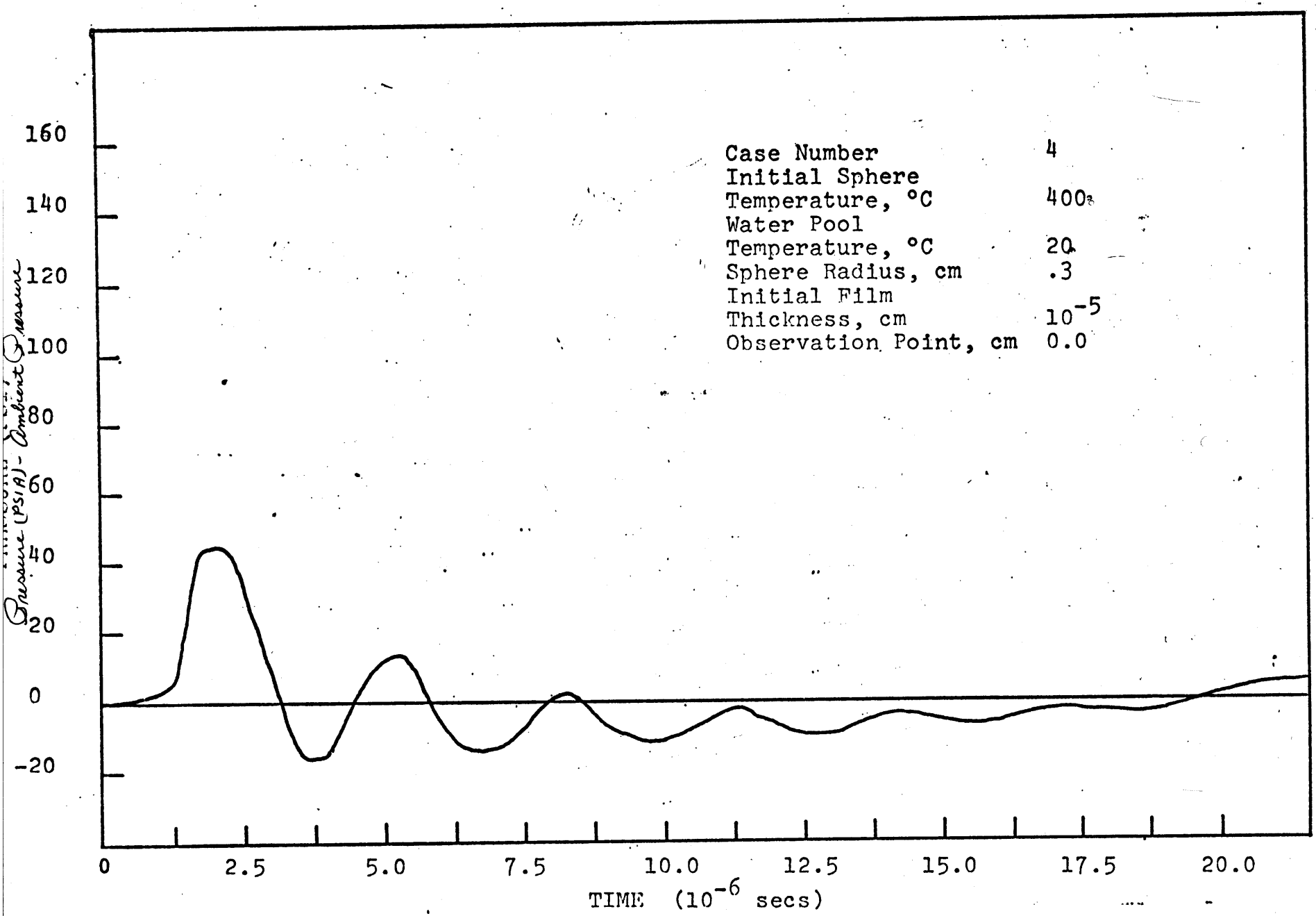
Case Number 4
Initial Sphere Temperature, °C 400
Water Pool Temperature, °C 20
Sphere Radius, cm .3
Initial Film Thickness, cm 10^{-5}
Observation Point, cm 0.0
Pressure (PSIA) - Ambient Pressure
160
140
120
100
80
60
40
20
0
-20
0
2.5
5.0
7.5
10.0
12.5
15.0
17.5
20.0
TIME (10^{-6} secs)

FIGURE 3.11

Pressure time history for Case 1
T_{ℓ}=20°C

FIGURE 3.11

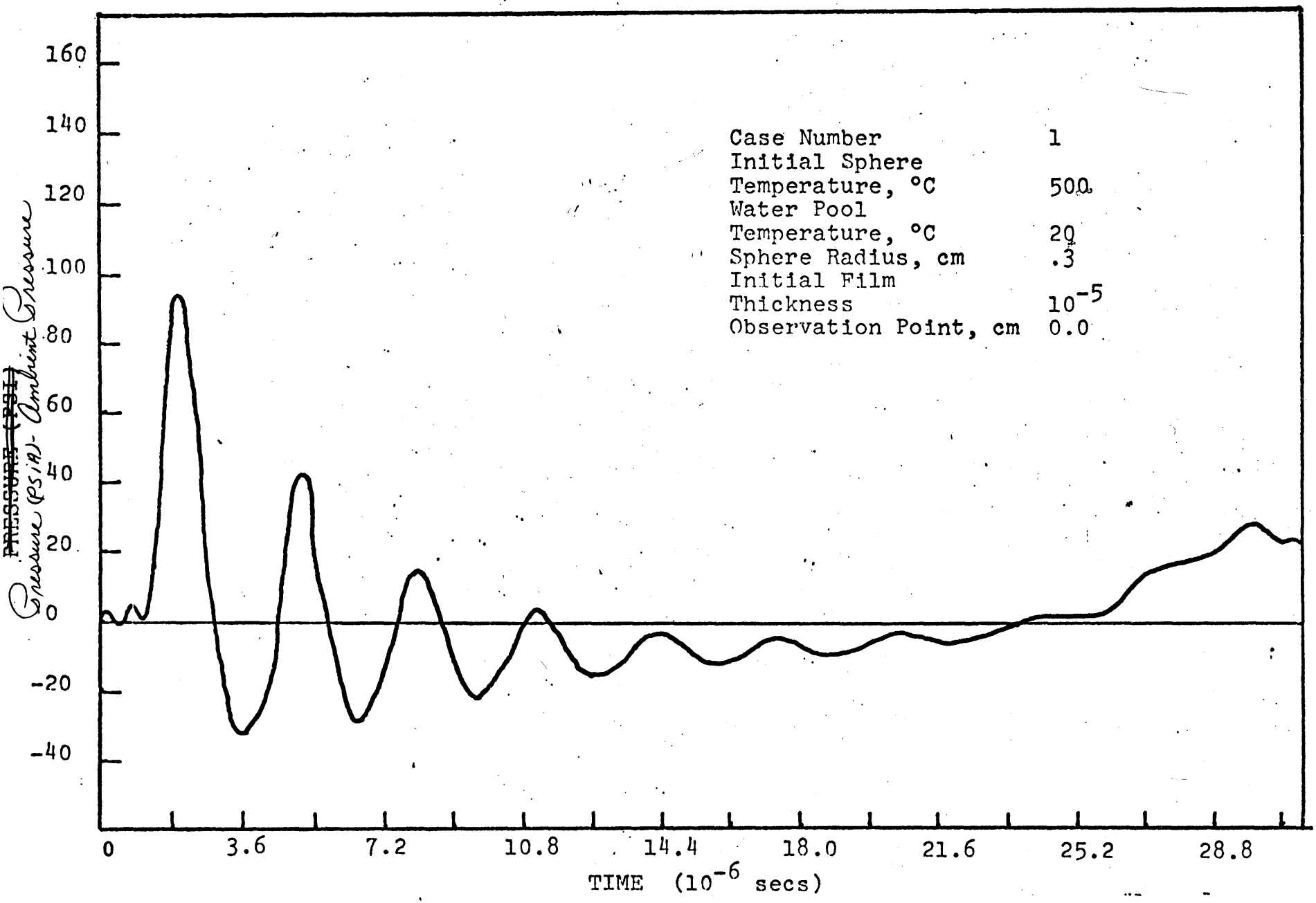
Case Number 1
Initial Sphere Temperature, °C 500
Water Pool Temperature, °C 20
Sphere Radius, cm .3
Initial Film Thickness 10^{-5}
Observation Point, cm 0.0
Pressure (PSIA) - Ambient Pressure
160
140
120
100
80
60
40
20
0
-20
-40
0
3.6
7.2
10.8
14.4
18.0
21.6
25.2
28.8
TIME (10^{-6} secs)

FIGURE 3.12

Pressure time history for Case 2
T_ℓ=50°C

FIGURE 3.12

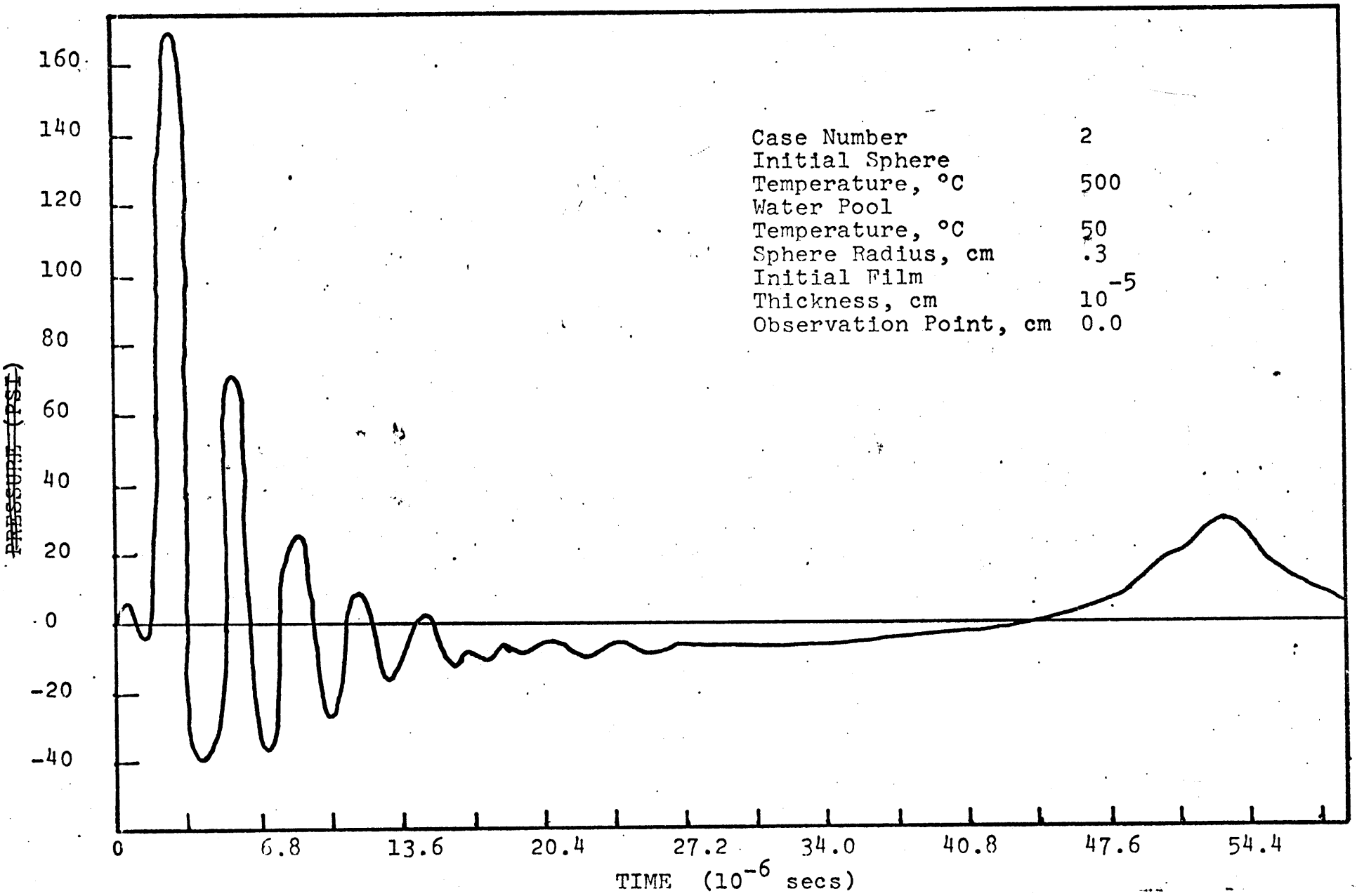
Case Number 2
Initial Sphere Temperature, °C 500
Water Pool Temperature, °C 50
Sphere Radius, cm .3
Initial Film Thickness, cm 10^{-5}
Observation Point, cm 0.0
PRESSURE (PSI)
160
140
120
100
80
60
40
20
0
-20
-40
0
6.8
13.6
20.4
27.2
34.0
40.8
47.6
54.4
TIME (10^{-6} secs)

FIGURE 3.13

Pressure time history for Case 3
T_ℓ=80°C

FIGURE 3.13

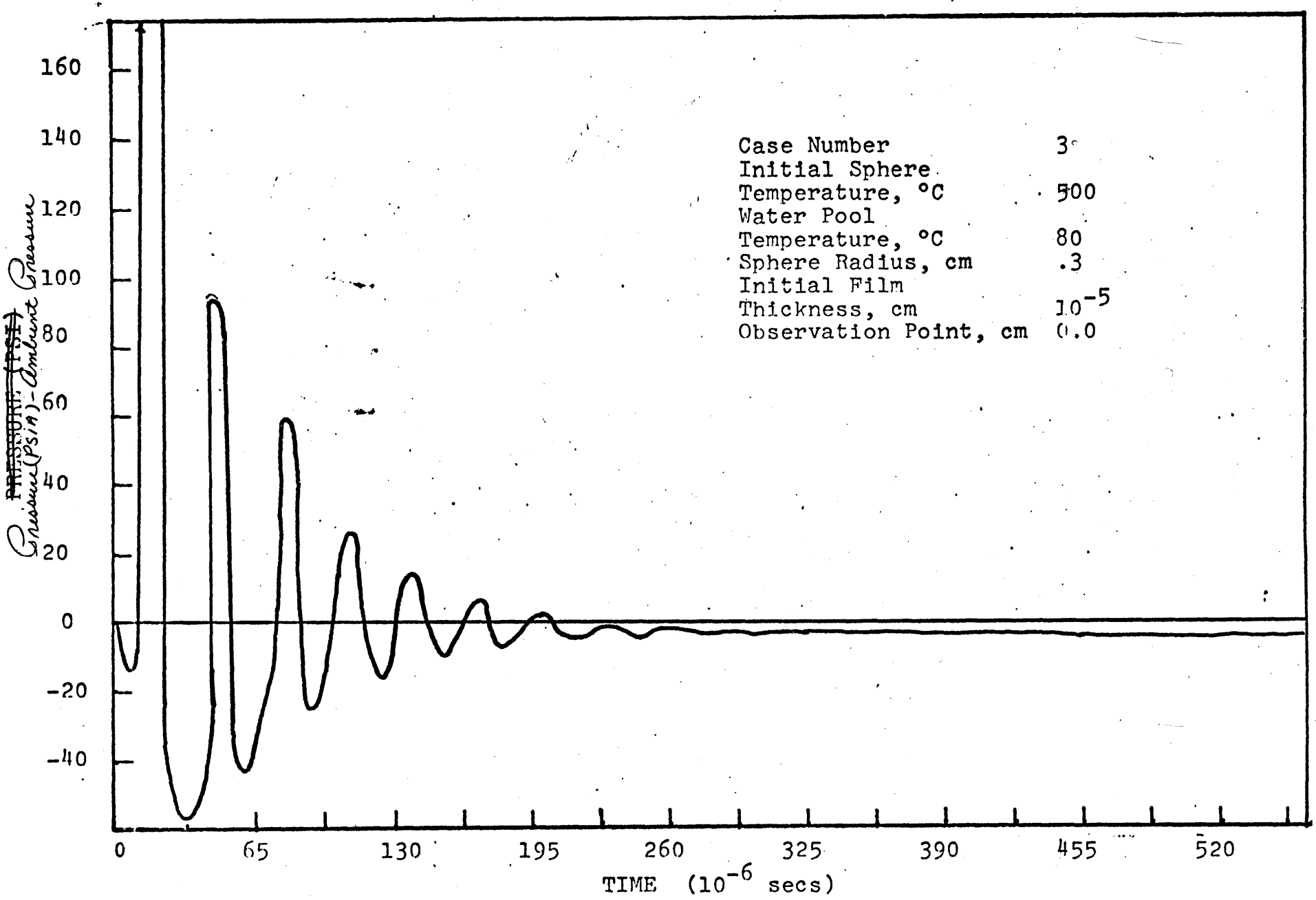
Case Number 3
Initial Sphere Temperature, °C 500
Water Pool Temperature, °C 80
Sphere Radius, cm .3
Initial Film Thickness, cm 10^{-5}
Observation Point, cm 0.0
Pressure (PSIA) - Ambient Pressure (PSIA)
160
140
120
100
80
60
40
20
0
-20
-40
0
65
130
195
260
325
390
455
520
TIME (10^{-6} secs)

CHAPTER IV

CONCLUSIONS

CHAPTER IV

CONCLUSIONS

In this chapter we would like to take up two topics. One is the conclusions which can be gained from the overall approach used and the second is the question of which approximations should be improved and what further work can be done to improve our understanding of the fragmentation phenomenon.

IV.1 Summary

First we discuss the conclusions which can be made. We have made the observation earlier in Chapter I that the phenomena is characterized by an oscillatory vapor film growth which experimentally can lead to an explosion. The Kazimi model can predict this oscillatory behaviour but it uniformly predicts minimum pressures at the surface which are well above the vapor pressure of the hot globule and do not by themselves predict the growth of a vapor bubble on the interior which would lead to a violent explosion. It was thought that since the solution to the wave equation has an inverse r dependance that the dependance would lead to much more negative pressure swings at $r = 0$ and would therefore lead to a mechanism for bubble growth and subsequently a large vapor explosion. This has not materialized for a variety of reasons which we will list.

First it should be noted from equation (3.25) that the interior solution is proportional to $\frac{\sin kr}{kr}$. This function does not blow up at zero and in fact the irregular solution was discarded as being unphysical for that reason. Second, the physical situation can be described qualitatively as being most nearly a driven resonant cavity (although there is no rigid wall and hence some transmission of the acoustic wave into the vapor film) and not a point source for which the earlier assumptions would be correct. A driven cavity however offers some possibilities for amplifying the pressure wave at the surface as it progresses to the interior. This approach was investigated and it was found that the initial pulse of short duration ($2*10^{-6}$ seconds) caused a transient response which was characterized by strong oscillations both positive and negative (also of short duration) which died out in time. However the longer duration portions of the surface wave were not affected because the frequency Fourier components which made them up were outside the resonance region. Thus there is no reason to expect vaporization on the interior in this model except for the very short time intervals mentioned earlier.

IV.2 Recommendations for Future Work

Next we discuss further work to improve the model.

From our discussion of viscosity effects in Chapter II it should be clear that this is not the largest energy loss mechanism in the system and in fact it is thought that if the rigid wall approximation were not made the coupling of the oscillations of the hot globule to the vapor film would cause much larger losses (radiation losses). Second the acoustical coupling should be quite large when the film is small (initially) and should become less and less as the film grows. This would mean that a smaller convergence factor could be used (10^{-6} instead of 10^{-2}) but the losses would still be quite large because of transmission losses in the beginning. As the film grows however the transmission losses will get smaller and the lower frequencies will be amplified much more because of the smaller convergence factor. We will outline a method by which these ideas can be implemented.

First we note that if there is to be some transmission out of the sphere, the boundary condition $G_\omega = 0$ must be dropped. In this case however, to calculate the additional contribution due to the driven motion of the surface, it is apparent from inspection of (3.12) we must know $(\frac{\partial p}{\partial r})_a$ as a function of time. Since we expect the transmission losses to be reasonably small we can use (3.25) to obtain

(4.1)

$$\frac{\partial p}{\partial r}(a,t) = \int_{-\infty}^{\infty} (\cot ka - \frac{1}{a}) \frac{a}{r} \frac{\sin kr}{\sin ka} p_{\omega}(a) e^{-i\omega t} dt \tag{4.1}$$

Next we can obtain $G_{\omega}(a)$ by applying the boundary conditions

$$G_{\omega 1}(a) = G_{\omega 2}(a) \tag{4.2}$$

$$G'_{1r}(a) = G'_{2r}(a) \tag{4.3}$$

and

$$G_2(R_\delta) = G_3(R_\delta) \tag{4.4}$$

$$G'_{2r}(R_\delta) = G'_{3r}(R_\delta) \tag{4.5}$$

where the subscripts 1, 2, and 3 refer respectively to the hot globule, the film, and the coolant regions. The equations can be solved to find the various reflection and transmission coefficients and thus determine $G\omega_1(a)$. Using this result, p_{ω} can be recomputed by adding on the additional surface term and the pressure found by doing the inverse transformation. Thus in effect, we are finding the fluctuating component of the pressure and the velocity in the film by knowing the effects of the film on the hot liquid. To the extent that the change in the pressure in the film caused by the motion of the surface

of the hot liquid is small (it is because of poor acoustic impedance matching between the film and the hot liquid, furthermore, the liquid is relatively incompressible), this is a good approximation. If higher precision is desired one could iterate the solution.

Finally we come to the question of the validity of using equation K4.17 in Kazimi's thesis to eliminate the vaporization rate as a variable. We begin by noting that equation K4.17 is used to eliminate the vaporization rate in K4.23 and K4.24 in the Kazimi model. However, K4.17 depends through K4.16b on $T_{\ell v}$ and through K4.8b on T_R. Now both T_R and $T_{\ell v}$ are not known until after the simultaneous solution of K(4.7, 4.9, 4.15, 4.23, 4.24, 4.27 and 4.38). It seems clear that the evaporation rate and the heat flow rates should be part of the set of simultaneous equation which are ultimately solved. It is our opinion that K4.17 leads to a minimum value for the vaporization rate and as a consequence the film thickness calculated are too small. In the cases calculated, the film thickness is only of the order of 10^{-3} cm which seems small in comparison with visual observation of ANL films in comparable situations. It may be that if $T_{\ell v}$ and T_R are changing slowly enough for the time intervals used the equation K4.17 is a reasonable approximation.

The period in time which is most sensitive is during the initial positive going pulse and effects could be expected to be largest there. If the integration time steps can be chosen small enough during this time the method used may be adequate.

```
      COMPLEX*8 CAT1(2000),CAT2(2000),FAC,ARGR,ARGA,XK(2000),XI,ONE,CX
     1,CAT3(2000),XY,AA
      REAL*4 P( 200),TIM( 200),FREQ
      REAL*4 WORK(4000)
      INTEGER*4 NN(1),NDIM,ISIGN,IFORM
       TPI = 2.0*3.14159
      ONE=(1.0,0.0)
      XI=(0.0,1.0)
C C IS VELOCITY OF SOUND IN MEDIUM IN CM/SEC     AND A(RADIUS) IS IN CM.
C N IS NUMBER OF DATA POINTS
C N MUST BE AN EVEN NUMBER  BECAUSE OF SIMPLE ALIASING METHOD USED
C NM IS NUMBER OF PRESSURE PTS. AND IS ANY INTEGER LESS THAN OR EQUAL TO 256
C T IS MAXIMUM VALUE OF TIM(E) IN UNITS OF TSCALE.
C DF IS DELTA FREQ
C XK IS WAVE NUMBER
   21 CONTINUE
      READ(5,100) NM,N,T,C,TSCALE,PINF,A,EPS
      WRITE(6,100) NM,N,T,C,TSCALE,PINF,A,EPS
      DO 10 II=1,NM,4
      JJ=II+3
      READ(5,101) (P(I),TIM(I),I=II,JJ)
      WRITE(6,103) (P(I),TIM(I),I=II,JJ)
   10 CONTINUE
      DO 8 I=1,NM
      J=NM-I+2
      JJ=J-1
      P(J)=P(JJ)
      TIM(J)= TIM(JJ)
    8 CONTINUE
      P(1)=PINF
      TIM(1)=0.0
      NMP1=NM+1
      DO 7 I=1,NMP1
      P(I)= P(I)-PINF
    7 CONTINUE
      WRITE(6,103) (P(I),I=1,NMP1)
```

```
      XN=N-1
      DT=T/XN
      CF=XN/(T*TSCALE*(XN+1.))
      TPDT=DT/TPI
C INTERPOLATION TO GET NUMBER OF DATA PTS. A POWER OF TWO
      DAT2(1)=P(1)
      M=2
      DO 1 I=2,N
      XJ=I-1
      XT=XJ*DT+TIM(1)
      DO 4 K=M,NMP1
      IF(XT-TIM(K)) 5,5,4
    5 KK=K-1
      JK=K
      GO TO 6
    4 CONTINUE
    6  DLT=TIM(JK)-TIM(KK)
       DAT2(I)=(P(KK)+(XT-TIM(KK))*(P(JK)-P(KK))/DLT)
      M=KK
    1 CONTINUE
      WRITE(6,104)
      WRITE(6,102)(  DAT2(I),I=1,N)
      NDIM=1
      NN(1)= N
      ISIGN=-1
C  THE FORWARD TRANSFORM
      IFORM=0
C IFORM=0 FOR DATA REAL
      CALL FOURT(DAT2,NN,NDIM,ISIGN,IFORM,WORK)
      WRITE(6,104)
      WRITE(6,102) (  DAT2(I),I=1,N)
      N2=N/2
      XNORM=N
      DO 23 I=1,N
      DAT2(I)=DAT2(I)/XNORM
   23 CONTINUE
```

```
      N5=N2+1
      DO 2 J= 1,N5
       XJ=J-1
       FREQ    =DF*XJ
       CX= FREQ    *TPI/C
       XK(J)=CX*(CNE-XI*EPS)
    2 CONTINUE
      WRITE(6,104)
      WRITE(6,102) (  DAT2(I),I=1,N5)
      WRITE(6,106)
      WRITE(6,102) (XK(II), II=1,N5)
      WRITE(6,105)
      WRITE(6,111) DF,DT
       AA=A*CNE
      DO 20 K=1,6
       XJ=K-1
       XP=XJ/5.0
      DO 9 I=1,N5
       ARGR=XP*XK(I)*AA
       ARGA= XK(I)*AA
       FREQ=XK(I)
       IF(FREQ    .EQ.0.0) GO TO 11
      GO TO 15
   11 FAC= CNE
      GO TO 13
   15 IF(K.EQ.1) GO TO 17
      GO TO 18
   17 FAC=ARGA/CSIN(ARGA)
      GO TO 13
   18 FAC=CSIN(ARGR)/CSIN(ARGA)/XP
   13 DAT3(I)= DAT2(I)*FAC
    9 CONTINUE
       WRITE(6,110)
       WRITE(6,102)(DAT3(I),I=1,N5)
C ALIASING THE TRANSFORM
       N3=N2+2
```

```
      N4=N+1
      DO 24 I=N3,N4
       DAT3(I) =(0.0,0.0)
   24 CONTINUE
      DO 22 J=1,N
       DAT1(J)=DAT3(J)
       JK=N -J+2
       XY=DAT3(JK)
       XY=CONJG(XY)
       DAT1(J)=DAT1(J)+XY
   22 CONTINUE
       DAT1(N5)=DAT1(N5)/2.0
      WRITE (6,109)
      WRITE(6,102) (DAT1(J),J=1,N )
       ISIGN=+1
       IFORM=+1
       NN(1)=N
C IFORM=+1 FOR A COMPLEX FUNCTION(DATA)
C  THE INVERSE TRANSFORM
       CALL FOURT(DAT1,NN,NDIM,ISIGN,IFORM,WORK)
       WRITE(6,107)
       WRITE(6,102)(  DAT1(I),I=1,N )
   20 CONTINUE
      GO TO 21
  100 FORMAT (2I5,3E10.3,3F10.4)
  101 FORMAT (8(E10.4))
  102 FORMAT(10(1X,E12.6))
  103 FORMAT (8(4X,E10.4))
  104 FORMAT(1H ,4HDATA)
  105 FORMAT(1H ,10H DF AND DT)
  106 FORMAT(1H ,2HXK)
  107 FORMAT(1H ,13HDATA PRESSURE)
  109 FORMAT(1H ,15HFINAL TRANSFORM)
  110 FORMAT(1H ,4HDAT3)
  111 FORMAT(2(5X,E12.6))
      END
```

APPENDIX B

SURVEY OF THE FAST FOURIER TRANSFORM AS APPLIED TO THE COMPUTATION OF FOURIER INTEGRALS

The solution of the acoustic wave equation as accomplished in this thesis is an example of the use of the Fourier transform over the infinite time domain. Computationally, however, we are interested only in finite time intervals so it is necessary to establish the connection between the finite Fourier transform at discrete intervals and the continuous transform over an infinite interval. Suppose we have a function $\chi(t)$ which has a F.T.

$$a(f) = \int_{-\infty}^{\infty} \chi(t) e^{-2\pi i f t} \, dt \tag{B.1}$$

Then

$$\chi(t) = \int_{-\infty}^{\infty} a(f) e^{2\pi i f t} \, df \tag{B.2}$$

If $\chi(t)$ is sampled at intervals of length Δt, then (2) expressed at the points $j \cdot \Delta t$, $j = 0, \pm 1, \pm 2, \ldots$ can be written

$$\chi(j \cdot \Delta t) = \int_{-\infty}^{\infty} a(f) e^{2\pi i j f / F} \, df \tag{B.3}$$

where $1/F = \Delta t$ or $F = 1/\Delta t$. This F is twice the Nyquist frequency. This integral can be broken up

into a sum identical with (B.3)

$$\chi(j \cdot \Delta t) = \sum_{k=-\infty}^{\infty} \int_{kF}^{(k+1)F} a(f) e^{2\pi ijf/F} \, df \qquad (B.4)$$

Now

$$\int_{kF}^{(k+1)F} a(f) e^{2\pi ijf/F} \, df = \int_{o}^{F} a(f+kF) e^{2\pi ij(f+kF)/F} \, df \qquad (B.5)$$

but

$$e^{2\pi ij(f+kF)/F} = e^{2\pi ijf/F} \qquad (B.6)$$

i.e. it is a function of period F.

So

$$\chi(j \cdot \Delta t) = \sum_{k=-\infty}^{\infty} \int_{o}^{F} a(f+kF) e^{2\pi ijf/F} \, dF \qquad (B.7)$$

$$= \int_{o}^{F} a_p(f) \, e^{2\pi ijf/F} \, dF \qquad (B.8)$$

where

$$a_p(f) = \sum_{k-\infty}^{\infty} a(f+kF) \qquad (B.9)$$

The subscript p on a function will denote the periodic function formed by the superposition of the nonperiodic function shifted by all multiples of a fundamental period. The function $a_p(f)$ is said to be an "aliased" version of a(f), with the aliasing occurring relative to the Nyquist frequency F/2.

Since $a_p(f)$ is a periodic function of f it has a Fourier series expansion. Further, we see from (B.8) that the coefficients of this expansion are given by 1/F times the sequence $\chi(j \cdot \Delta t)$. Hence, (B.8) has the reciprocal equation

$$a_p(f) = \frac{1}{F} \sum_{j=-\infty}^{\infty} \chi(j \cdot \Delta t)\, e^{-2\pi i f j/F} \qquad \text{(B.10)}$$

In this relationship between $a_p(f)$ and $\chi(j \cdot \Delta t)$ the usual roles of time and frequency are interchanged; i.e., a periodic, continuous function of frequency corresponds to a sequence of time coefficients. Now, (B.10) is a discrete Fourier transform but it is not finite. However, if we consider the values of $a_p(f)$ at N equally spaced points between 0 and F, i.e. sample $a_p(f)$ at intervals $F = F/N = 1/(N\Delta t)$, we obtain

$$a_p(n\Delta f) = \frac{1}{F} \sum_{j=-\infty}^{\infty} \chi(j\Delta t)\, e^{-2\pi i j n/N}$$

$$= \frac{1}{F} \sum_{j=0}^{N-1} \left\{ \sum_{\ell=-\infty}^{\infty} \chi(j\Delta t + \ell N \Delta t) \right\} e^{-2\pi i j n/N} \qquad \text{(B.11)}$$

The last result follows from the fact that $e^{-2\ ijn/N}$ is a periodic sequence of j with period N. Hence we finally have

$$a_p(n\Delta f) = \frac{1}{F} \sum_{j=0}^{N-1} \chi_p(j\Delta t)\, e^{-2\pi ijn/N} \qquad \text{(B.12)}$$

where

$$\chi_p(t) = \sum_{\ell=-\infty}^{\infty} \chi(t + \ell T) \qquad \text{(B.13)}$$

is periodic of period $T = N\Delta t = 1/\Delta f$.

It is only a matter of a multiplication constant to put (B.12) in the form of the finite Fourier transform. Thus, if two functions are Fourier transforms of one another then the sequences obtained from them by sampling and aliasing in this fashion are finite Fourier transforms of one another.

REFERENCES

1. C. N. Kelber et al., "Safety Problems of Liquid-Metal-Cooled Fast Breeder Reactors", ANL-7657, Feb. 1970.

2. J. E. Bovier, et al., "The Vapor Explosion - Heat Transfer and Fragmentation. I. Introduction to Explosive Vapor Formation", Technical Report No. ORO-3936-1, Nov. 1969.

3. M. S. Kazimi, "Theoretical Studies on Some Aspects of Molten Fuel-Coolant Thermal Interaction", Ph.D. Thesis, MIT (1973)

4. D. Armstrong and D. Cho, "LMFBR Nuclear Safety Program Annual Report", ANL-7800, 340-358, July 1971.

5. L. C. Witte, et al., "The Vapor Explosion - Heat Transfer and Fragmentation. IV. Rapid Quenching of Molten Metal" Technical Report No. ORO-3936-6, Aug. 1971.

6. P. M. Morse and I. Ingard, "Theoretical Acoustics", McGraw Illl, 1968.

7. Cooley, James W. and John W. Tukey, An Algorithm for the Machine Calculation of Complex Fourier Series", Mathematics of Computation, Vol. 19 (April, 1965) p. 297 - 301.

8. Brenner, Norman, "FOURT" MIT Information Processing Center Applications Program Series Report, AP-7 revision 4.